Master's Thesis

Study on Optimal Device Design for 2-terminal Mechanical Perovskite/Silicon Tandem Solar Cells with Transparent Conductive Adhesives

In Young Choi

Department of Materials Science and Engineering

Graduate School of UNIST

2019

Study on Optimal Device Design for 2-terminal Mechanical Perovskite/Silicon Tandem Solar Cells with Transparent Conductive Adhesives

In Young Choi

Department of Materials Science and Engineering

Graduate School of UNIST

Study on Optimal Device Design for 2-terminal Mechanical Perovskite/Silicon Tandem Solar Cells with Transparent Conductive Adhesives

A thesis
submitted to the Graduate School of UNIST
in partial fulfillment of the
requirements for the degree of
Master of Science

In Young Choi

12. 18. 2018

Approved by

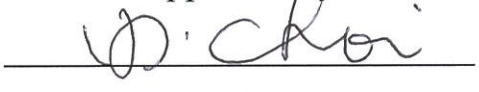

Advisor
Kyoung Jin Choi

Study on Optimal Device Design for 2-terminal Mechanical Perovskite/Silicon Tandem Solar Cells with Transparent Conductive Adhesives

In Young Choi

This certifies that the thesis of In Young Choi is approved.

12. 18. 2018

signature

Advisor: Kyoung Jin Choi

signature

typed name: Myoung Hoon Song

signature

typed name: Hyesung Park

Abstract

To overcome the theoretical efficiency limit of silicon solar cell, researches on tandem solar cells have been actively carried out. However, most studies focus on developing the deposition technique and SHJ silicon-based tandem which need high-cost. Here, for the first time, the low-cost 2-terminal mechanical silicon/perovskite tandem devices is developed by using the transparent conductive adhesive (TCA). TCA consists of Ag-coated Poly(methyl 2-methylpropenoate) particles which make electrically lossless with low contact resistance of $5.46 \times 10^{-2}\ \Omega \cdot cm^2$ and transparent adhesives, Norland optical adhesives, which attach the two sub cells mechanically stiff. Especially since TCA layer is tens of micro-scale and flexible, the commercial Al-BSF silicon solar cell with the textured surface can be easily applied for the tandem devices unlike existing monolithic tandem devices that required additional processes. Based on optimized design though optical simulation, the 2-terminal mechanical tandem solar cells with the current density of 15.43 mA/cm^2 and steady-state PCE of 19.40% are demonstrated. This result is the highest efficiency among the Al-BSF silicon-based tandem devices. In the commercialization viewpoint, our tandem devices are promising because a large-area cell can be achieved with low TCA resistance even in large-area and it is encapsulation-freely stable in humid condition (100h in RH 85%).

Contents

List of Figures

List of Tables

I. Introduction

Solar cell technology is evolving into solar cells that increase efficiency, reduce cost, or have special functions such as transparent or flexible solar cells. Silicon solar cell technology, which has a market share of about 93%[1] of the entire solar cell market, has a wide spectrum of BSF, PERC, HIT and IBC in terms of efficiency and price. For example, the efficiency of an IBC cell has been reported to be as high as 26.6%[2], close to the theoretical limit of 28%[3], and the price of a BSF cell is less than 0.2 $/Wp, which is the lowest among all solar cells. However, it is difficult to meet the efficiency and price of silicon solar cell at the same time, and breakthrough technology is needed to overcome it. Among these breakthrough technologies, the most promising technique is a tandem cell strategy in which two or more solar cells with different band gap energies are stacked[4-6]. In particular, perovskite solar cells are suitable for tandemization with silicon solar cells because the band gap of the perovskite layer can be controlled[7]. Because it has a steep absorption edge[8], a high absorption coefficient and a long carrier diffusion length[9], the efficiency is increased at a high speed for a short period of time to over 23%[2]. According to the simulation results, if the perovskite top cell with the bandgap of 1.73 eV and the silicon bottom cell form a tandem configuration, a high-efficiency over 30% tandem device can be acheived[10-12]. Also, when expecting the levelized cost of electricity of the perovskite/silicon tandem device, it can be reduced about 5% compared to the conventional silicon solar cells[13]. Therefore, it is very competitive as next generation-commercial solar cells.

The representative configurations of tandem devices include a 2-terminal monolithic and a 4-terminal mechanical configuration. The 4-terminal mechanical tandem device, in which the bottom cell is operated by the light transmitted through the top cell, is electrically independent of the two sub-cells[14-16]. While there is no need for current matching technology and additional complicate process, it is difficult to be low-cost and high-efficiency due to their optical losses as well as electrical circuit complexity. On the other hand, in case of the 2-terminal monolithic tandem, two sub-cells are connected in series by using recombination layer[17-21]. Since the current matching and optimal recombination layer are required and the top perovskite solution process should be uniformly formed on the silicon surface, it is inevitable to change the conventional silicon cell structure to a new structure suitable for the tandem. If the current matching and losses recombination is realized, it can be a low-cost, high-efficiency cell. Therefore, much research has been carried out to balance the current density of two sub-cells. In particular, to enhance the relatively insufficient light absorption of silicon, the tandem solar cells based on the textured silicon have been recently reported[22]. However, when the top perovskite cell process is formed on the textured silicon surface by the existing solution process, unconformal coating problem occurs[23]. To deposit uniform top layers on the textured surface, nowadays vacuum depositing techniques

for the top perovskite cell are being studied as a solution. For example, the 25.2% of monolithic tandem solar cells with all-vacuum depositing technique was reported by Ballif et.al[20]. However, vacuum deposition technology is not only expensive, but also requires time for new process conditions.

In addition to these two representative configurations, there is a 2-terminal mechanical tandem device. After the top and bottom cells are fabricated individually, a series connection is formed by mechanical connection of their electrodes. Each sub-cells can be individually operated as a four-terminal tandem device or be mechanically and electrically connected to operate as a two-terminal tandem device. Ito group has reported 2-terminal mechanical tandem device with 15.2% efficiency by mechanically contacting ITO electrode of c-Si bottom cell and IZO electrode of perovskite top cell[24, 25]. However, it cannot be regarded as a perfect device structure because the two sub-cells was attached and measured using a scotch tape and a spring needle.

Here, we firstly developed a perfect one body of 2-terminal mechanical silicon/perovskite tandem devices by using optically transparent and electrically conductive adhesive. The transparent conductive adhesive (TCA) consists of Ag-coated Poly(methyl 2-methylpropenoate) (PMMA) particle which make conductive in out of plane direction and transparent adhesive, norland optical adhesives (NOA), which connect the two sub cells mechanically. Since TCA is tens of micro-scale and flexible, conventional silicon solar cell with textured surface can be directly applied for the fabrication of tandem devices without further modification to the existing silicon solar cell process. Therefore, commercialized Al-BSF cells with textured substrates can be used without any other expensive vacuum deposition techniques, and that enables the realization of low-cost, high-efficiency cells. Based on optimized design expected by the optical simulation, we successfully fabricated the 2-terminal mechanical perovskite/commercial Al-BSF silicon tandem solar cells with the current density of 15.48 mA/cm^2 and steady-state PCE of 19.4%.

II. Theoretical Development

2-1. Principle of tandem solar cells

Among the various types of solar cells, silicon-based solar cells have been researched for a long time. At present, the efficiency of the heterojunction silicon cell have been achieved to 26.6%, which is close to the theoretical efficiency limit. In addition, commercial large area Al-BSF and PERC silicon solar cells are produced with a performance over 20% efficiency. However, since the single junction solar cells can absorb only a limited region of solar spectrum, their efficiency cannot exceed over 30% due to large amount of the below band gap absorption loss and thermalization loss[5], as shown in Figure 1. On the other hand, if the top cell with a large bandgap and the bottom cell with a small bandgap are combined as a tandem, the high efficiency over 30% is enable. It is because the top cell with a large bandgap absorbs the light of a short-wavelength region and the bottom cell with a small bandgap absorbs light of a long-wavelength region, reducing the below band gap absorption loss and thermalization loss. Therefore, in order to demonstrate low-cost, high-efficiency solar cells, tandem structure is a very promising technology.

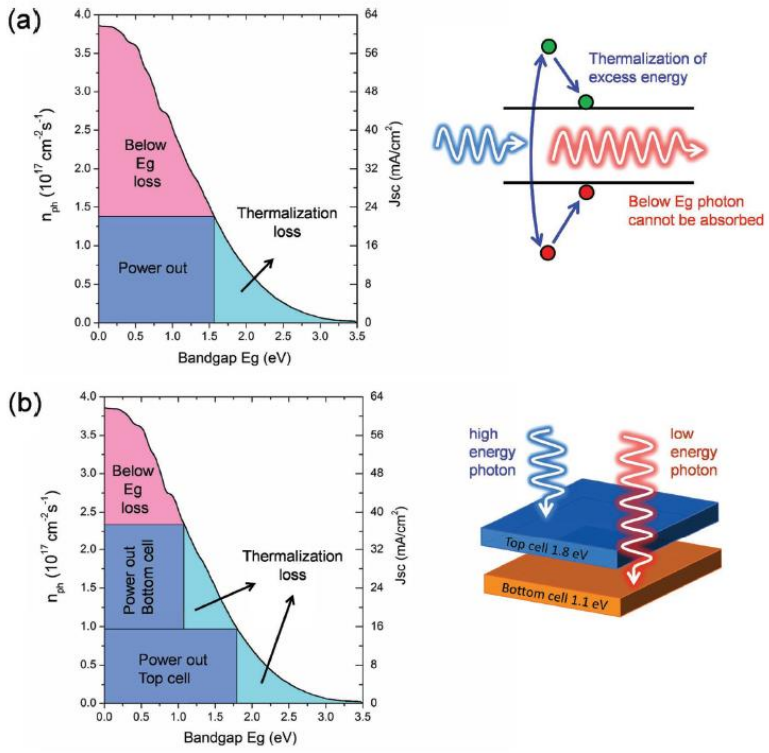

Figure 1. Losses of (a) a single-junction solar cell with the bandgap of 1.55 eV and (b) dual-junction[5] tandem solar cell with 1.8 eV bandgap top cell and 1.1 eV bandgap bottom cell.

2-2. Representative configurations of tandem solar cells

The representative configurations of tandem devices include a 4-terminal mechanical, a 2-terminal monolithic and 2-terminal mechanical configuration, as you can see in Figure 2. In case of the 4-terminal mechanical tandem structure, in which the bottom cell is operated by the light transmitted through the top cell, two sub-cells are electrically independent. Many studies have been made on the fabrication of transparent electrodes with high transmittance and the minimization of parasitic absorption. For example, 26.9% of 4-terminal tandem device using the high efficient PERL silicon bottom cell and highly transparent top cell with CuSCN for HTL and AgNW as transparent electrode was reported by Christoph et.al[26]. The 2-terminal monolithic tandem structure has a recombination layer on the top of the bottom cell and the layers for the top cell stacked on it, forming a series connection of two sub-cells. In this case, the current matching of two sub-cells and the optimal recombination layer are important points for high efficiency. The highest efficiency of monolithic tandem device was 25.2% reported by Ballif et.al[20]. The nc-Si recombination layer was formed on the textured silicon bottom cell to minimize reflection, and the perovskite top layers were vacuum deposited to form a uniform layer. The last one is 2-terminal mechanical tandem structure. After the top and bottom cells are fabricated individually, a series connection is formed by mechanical contact with transparent conductive adhesives. Each sub-cells can be individually operated as a 4-terminal tandem device or be mechanically and electrically connected to operate as a 2-terminal tandem device. Among the above tandem configurations, 2-terminal tandem configurations are more suitable for commercialization.

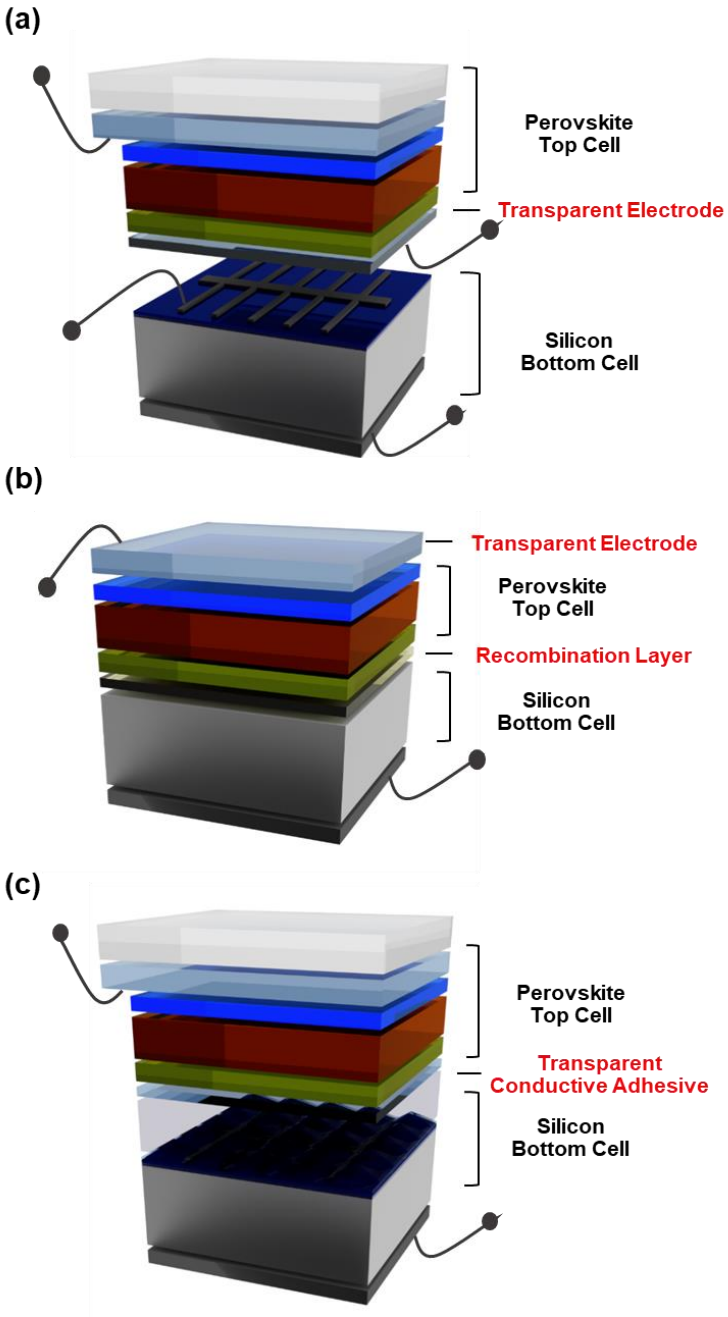

Figure 2. The schematics of (a) 4-terminal mechanical tandem, (b) 2-terminal monolithic tandem and (c) 2-terminal mechanical tandem.

2-3. Theoretical efficiency of tandem solar cells

As shown in Figure 3 which is from the simulation data of the reported paper, in case of 2-terminal tandem configuration, if a 1.12 eV E_g of silicon solar cells are tandemized with a 1.75 eV E_g perovskite solar cells, the high efficiency of 38% or more can be achieved[27]. According to this simulation data, many researches of tandem solar cells are carried out and recently, 25.2% of monolithic tandem solar cells have been reported. With this trends, high efficiency of over 30% is expected to be achieved in the near future.

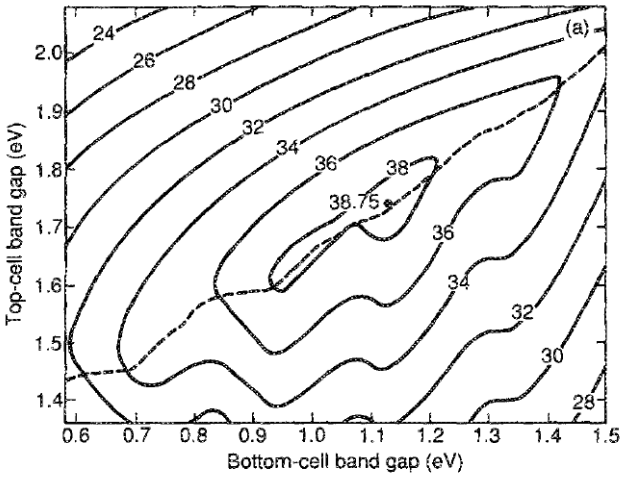

Figure 3. 2-terminal theoretical efficiency as a function of bandgap with optimized top-cell thickness[27].

III. Experimental Method & Materials

Fabrication of silicon bottom cells :

The silicon bottom cells were fabricated using the square pieces (15 mm×15 mm) of boron-doped 1-5Ω, 525 um thick Cz-Si wafer. In case of the pyramidal silicon solar cell, silicon surface was etched by KOH/IPA solution. After cleaning the Si substrate using acetone, IPA and DI water, 2 um-thick Al was deposited on the back side of the substrate by e-beam evaporation and a phosphorous SOD diffusant (SOD P507, Filmtronics) is spin-coated on the front side at 3000 rpm. For the simultaneous formation of Al-BSF and n-type emitter, the wafer was co-fired by using a rapid thermal annealing (RTA) at 900℃ in an N_2 atmosphere for 2 min. Then, phosphor-silicate glass (PSG) on the surface was removed by HF solution for 30s. Before depositing the passivation layer, the wafer was cleaned using the RCA1 and RCA2 process. A 70 nm-SiN_x passivating layer which has refractive index of 1.97 at the wavelength of 900 nm was deposited by plasma enhanced chemical vapor deposition (PEH-600, SORONA) at 350℃. (For edge isolation to make the active area exact, 5 mm×5 mm active area was isolated by ICP etch process.) For the top electrode, Ti/Ag grid pattern was formed through photolithography and lift-off process. A 1um Ag was finally deposited by e-beam evaporator for the back contact electrode.

Fabrication of the perovskite top cells :

A 70 nm thick dense TiO_2 layer was deposited on the patterned F-doped SnO_2 (FTO, TEC8, Pilkingon) substrate by spray pyrolysis at 450℃ using titanium diisopropoxide bis(acethylacetonate) solution (Sigma-Aldrich) diluted in ethanol. ~250 nm thick mesoporous TiO_2 layer was spin-coated on the bl-TiO_2/FTO substrate using the TiO_2 paste (SC-HT040 paste, Sharechem) diluted in 2-methoxyethanol and annealed at 450℃ for 1h on the hotplate. $MAPbI_3$ powder (TCI Chemicals) was diluted in N-N-dimethylformamide (Sigma-Aldrich) and dimethyl sulfoxide (Sigma-Aldrich) (1:4 v/v) at a various concentration at 60℃ and filtered by 0.45 um PTFE filter. Filtered $MAPbI_3$ solution was spin-coated onto the mp-TiO_2/bl-TiO_2/FTO substrate at 5000 rpm for 60s. During spin coating, toluene was drop-casted on that substrate in 10s to the start of the spinning process and then the film was dried at 100℃ for 10min on a hot plate. A 10mg poly(triarylamine) (PTAA, EM Index, M_w=17900gmol^{-1}) was diluted in toluene(1ml) and mixed with 10ul of a solution 170mg ml^{-1} lithium bistrifluoromethanesulphonimidate (Sigma-Aldrich) in acetonitrile and 7.5ul of 4-tert-butylpyridine. PTAA solution was spin-coated on the $MAPbI_3$/mp-TiO_2/bl-TiO_2/FTO substrate at 3000 rpm for 30s. For the opaque perovskite solar cell, 150 nm of Au was evaporated on the top of the PTAA film as the top electrode.

Tandem device fabrication :

For the semi-transparent perovskite top cell, 10 nm thick MoO_3 was deposited by e-beam evaporation with a ratio of 0.1 As^{-1} as a buffer layer and 150 nm thick IZO was deposited by RF-sputter at room temperature as the transparent electrode. Also, 30nm thick IZO was deposited on the top of the silicon solar cell to make the entire area electrically conductive. 0.5wt% of Ag-coated PMMA particles (PMPMS-AG-1.53, Cospheric, 45-53μm) was diluted in the transparent adhesive, Norland Optical Adhesive (NOA83H, Norland Products) and the TCA solution was mixed by Voltex Mixer (VW-10, DAIHAN Scientific). TCA solution was spin-coated on the IZO of the silicon solar cell at 3000rpm for 30s and TCA coated silicon solar cell was mechanically attached to the IZO layer of the perovskite top cell and annealed at 100℃ for 1h. The edges of their interface were sealed with the EVA film at 100℃ for 15min.The active area of the final tandem devices is 0.25 cm^2.

Optical Simulation for Si/Perovskite tandem solar cells :

The theoretical reflectance and internal light energy flux of the device were computed using the optical simulation which was implemented by a Python cross-platform software. For the tandem device with multilayers, a Generalized Scattering Matrix Method was used. All layers were treated coherently except only c-Si. The c-Si layer was treated incoherently due to its thickness of 525 um which is larger than the coherence length of sunlight. The values of the refractive index (n) and extinction coefficient (k) with the wavelength were measured using the ellipsometer (Elli-SE-UaM8, Ellipso technology Co., Korea) for each layer. The maximum current density was calculated by multiplication of the simulated internal light energy flux and the photon flux with the wavelength from 350 nm to 1200 nm through MATLAB software.

Fabrication of PDMS AR foil :

The square pieces (30 mm×30 mm) of silicon substrate was cleaned with acetone, IPA and DI water. The silicon native oxide on the silicon surface was removed by dipping into buffered oxide etchant (BOE, HF/NH_4F = 7:1) and the Si substrate was rinsed with DI water and dried by N_2 gas flow. First, Si substrate was immersed into potassium hydroxide solution (45wt% KOH) at 95℃ for 10min to remove the saw damage of the silicon surface. After rinsing the substrate, Si substrate was immersed into the solution mixed with KOH solution, IPA and DI water (8:5:100 v/v) at 70℃ for 40min to fabricate the micro-pyramidal silicon mold and rinsed with DI water and dried by N_2 gas flow. To fabricate the PDMS AR foil, PDMS solution (Sylgard 184, Dow Corning Co.) was spin-coated on the etched silicon mold at 3000 rpm and cured at 100℃ for 1h. Finally, the cured PDMS foil was peeled off from the silicon mold.

Measurements :

The morphology and thickness of perovskite film and TCA film were observed by a scanning electron microscopy (S-4800 Cold FE-SEM, Hitachi high-Technologies). The transmittance and absorbance of the perovskite films were measured using a UV-vis spectrometer (Cary 5000, Agilent Tec.). The power conversion efficiencies of all devices were measured under simulated AM 1.5G (100 mW/cm^2) with a xenon lamp solar simulator. *J-V* curves of the perovskite solar cells were measured by using a black aperture mask of 0.0921 cm^2 area and J-V curves of the silicon solar cells and tandem solar cells were measured by using a black aperture mask of 0.25 cm^2 area.

IV. Results and Discussion

4-1. Properties of the transparent conductive adhesives

Figure 4 shows the schematic of the 2-terminal mechanical perovskite/silicon tandem device. In this tandem structure with TCA, the fabrication processes of the conventional single cells were used as they are without changing. The detail fabrication process is described in the experimental section. The semi-transparent (ST) perovskite top cells were composed of FTO/bl-TiO_2/mp-TiO2/$MAPbI_3$/PTAA/MoO_3/IZO, as shown in Scanning electron microscopy (SEM) image of Figure 5. A 10 nm MoO3 thin film was used to protect MAPbI3 layer from the sputtering damage during IZO sputtering[28]. The 150nm thick IZO top electrode was deposited by RF-sputtering and its sheet resistance was 30 Ω/sq with 87% of transmittance. In case of the silicon bottom cells, the conventional Al-BSF silicon cell structure, Ag grid/SiN_x/n+ emitter/p-Si/Al-BSF/Al, was used. And thin IZO (30 nm) was deposited on top of the Ag grid pattern. This thin IZO layer makes the entire top area of silicon bottom cells laterally conductive. Thus, without this layer, Ag-coated PMMA particles in TCA cannot connect the two sub-cells effectively. If only IZO is on the silicon cell without Ag grid, IZO cannot effectively collect the charges separated from the junction and thus it makes the fill factor low. On the other hand, with Ag grid between IZO and the silicon, it forms the n-type ohmic contact, and improves the cell performance by facilitating the charge collection. Then the two sub cells were mechanically and electrically attached via TCA.

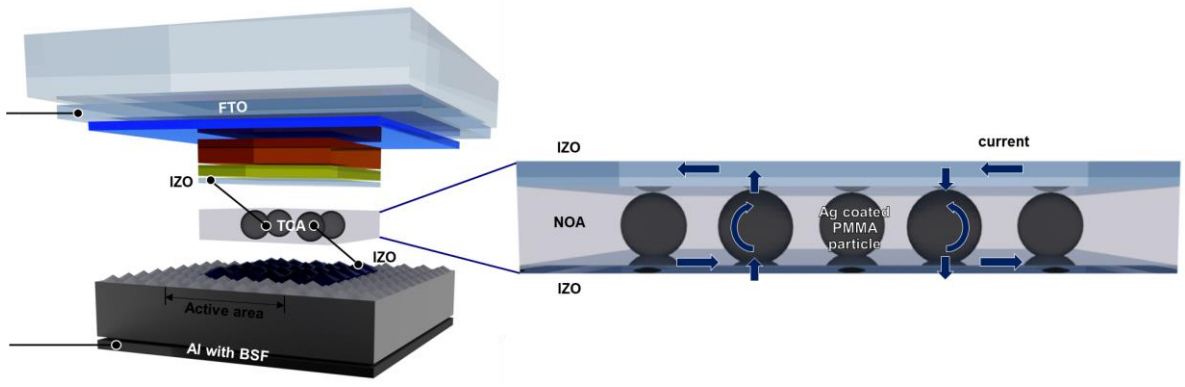

Figure 4. Schematic illustration of the 2-terminal mechanical perovskite/silicon tandem device with transparent conductive adhesives (TCA). (not to scale)

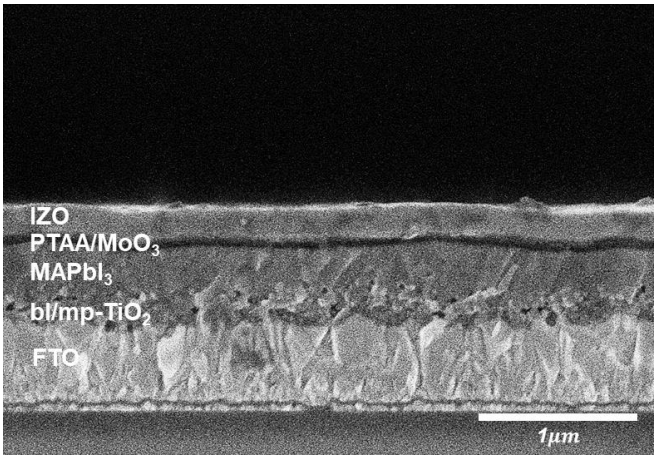

Figure 5. The cross sectional SEM image of semi-transparent perovskite top cell.

TCA consists of Ag coated PMMA particles and NOA. Ag coated PMMA particles electrically connect the top cell and bottom cell and NOA adhesive acts as an adhesive to mechanically attach the two cells. As the candidates for the transparent adhesives of TCA, there are NOA, poly(dimethylsiloxane) (PDMS), ethlyene-vinyl acetate (EVA) and so on. Among them, NOA adhesive has low viscosity to be easy to be coated on textured surface and is easy to handle because it maintains liquid state at RT in the dark. Also, compared with PDMS and EVA, NOA is suitable as a TCA material because it has excellent tensile strength and hardness when it is hardened by heat treatment (Table 1). In case of the PEDOT:PSS film[29, 30] and the graphene[31, 32], which have been mainly studied as a TCA, the lateral conductivity and transmittance is also good, but it cannot be applied in the textured surface because of its thin thickness. In contrast, our TCA with Ag-coated PMMS particle can be used without any problem on the textured surface because the soft and conductive micro-scale particles electrically connect the top cell and bottom cell in the direction of out of plane without loss. As you can see in the SEM image (Figure 6), our TCA solution conformally covers the textured silicon surface without any air gap with a thickness of 42um. Also, the 45um Ag-coated PMMA particles act as an electric bridge between them. If TCA can be applied to the textured silicon surface, it is strong advantage in terms of efficiency because the textured surface reduces the reflectance of light and enhance the light absorption compared to planar surface.

Table 1. The optical and mechanical characteristics of the transparent adhesives.

Polymer	NOA 83H	PDMS	EVA
Transmittance	good	good	Good
Refractive Index	1.56	1.42	1.48
Viscosity at RT	low	medium	High
Handling	easy (1 solution)	easy (2 solutions)	complicate
Tensile Strength	high	low	Low
Hardness	high	medium	low

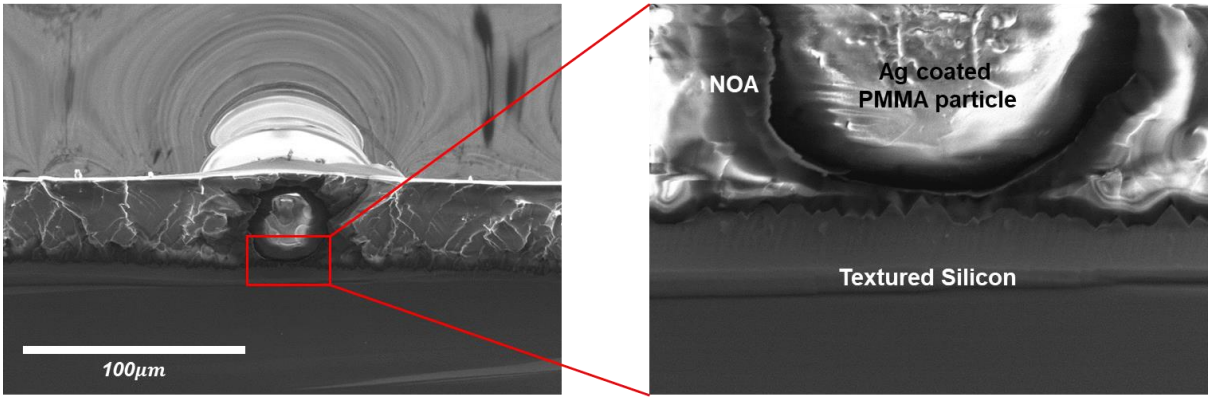

Figure 6. The cross-sectional SEM images of the TCA layer on the textured silicon surface. The thickness of the TCA is approximately 42μm and the height of the Ag coated PMMA particle is 45μm.

The electrical and optical properties of TCA depend on the concentration of Ag coated PMMA particles in TCA. In order to precisely measure the specific contact resistance of TCA ($r_{contact}$), TCA with various concentration was uniformly coated and cured between a 0.5 um thick Ag deposited glass and a 0.5 um thick Ag deposited planar silicon substrate[33]. Then the total resistance (R_{tot}) of this system was measured by four-point probe measurement method. In this system, it is assumed that the 0.5 um thick Ag electrode has no resistance. In fact, when comparing $\mathrm{r_{contact}}$ with the resistance of the 0.5 um thick Ag electrode obtained later, it was confirmed that there was five-order difference in their values. As shown in Figure 7a, *I-V* curves for all samples varying with TCA concentration reveal the ohmic contact behavior. The total resistance (R_{tot}) is defined by

$$\mathrm{R_{tot}} = \frac{V_{tot}}{I_{tot}} \quad (1)$$

$$\mathrm{R_{tot}} = \mathrm{R_{tip,1}} + \mathrm{R_{bulk,1}} + \mathrm{R_{contact}} + \mathrm{R_{bulk,2}} + \mathrm{R_{tip,2}} \quad (2)$$

$$r_{contact} = R_{contact} \times A_{contact} = \left[\sum_{i=1}^{N}(R_{particle,i})^{-1}\right]^{-1} \times A_{contact} \quad (3)$$

Where V_{tot} and I_{tot} are the applied voltage and the measured current, $R_{tip,1}$ and $\mathrm{R_{tip,2}}$ are the resistances from contact tips, $R_{con\_pad,1}$ and $R_{con\_pad,2}$ are the contact resistances of the Ag contact pad, $A_{contact}$ is the contact area, and $R_{particle}$ is the resistance of the one of the Ag-coated PMMA particle between Ag-deposited glass and Ag-deposited silicon. $R_{tip,1}$ and $R_{tip,2}$ are obtained by measuring *I-V* curve from tip to tip. $R_{con\_pad,1}$ and $R_{con\_pad,2}$ are estimated by y-intercept in the R_{tot}-$A_{contact}$ curves[34]. These sum value is $3.58 \times 10^{-2}\ \Omega$. R_{tot} can be calculated by equation (1) and $R_{contact}$ can be obtained by subtracting the above factors, as you can see in equation (2). As the concentration of TCA increases, the slope of the *I-V* curve is increased and the total resistance decreases gradually when the contact area is fixed to 0.25cm^2. It is because the conduction path increases as the number of Ag-coated PMMA particles increases[35, 36]. In addition, as the concentration of TCA increases, the coverage of the Ag-coated PMMA particles increases and the transmittance of TCA layer on glass which wavelength region is from 700nm to 1100nm decreases, as shown in Figure 7b. The wavelength region from 700nm to 1100nm was focused because the silicon bottom cell absorbed the most light in that region. It can be seen that the reflectance increases as the TCA concentration increases. The detail optical properties are in Figure 8.

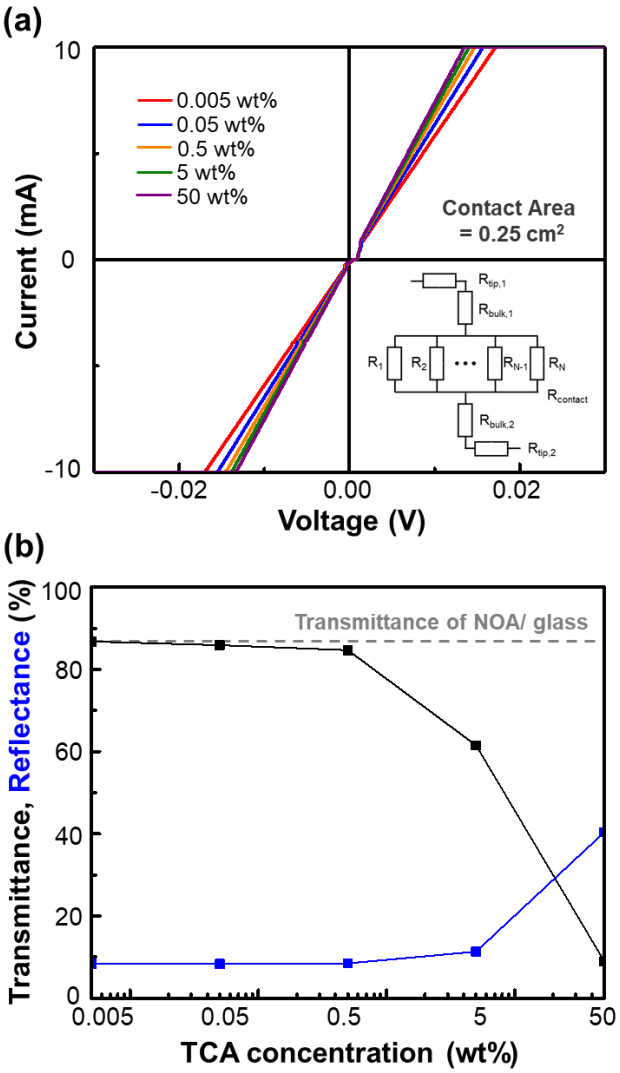

Figure 7. (a) I-V curve of the TCA layer between the Ag-deposited glass and the Ag-deposited planar silicon and (b) the average transmittance and reflectance of the TCA layer on glass as function of the concentration of TCA.

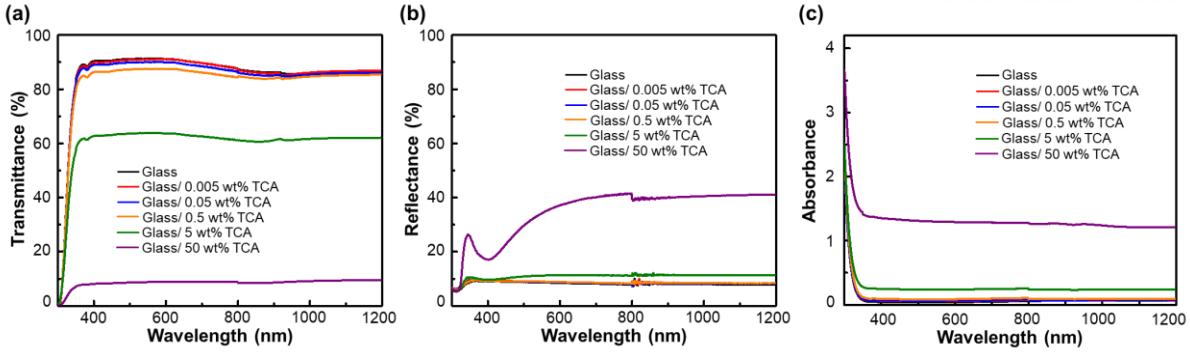

Figure 8. (a) Transmittance, (b) reflectance and (c) absorbance of the TCA on glass with varying the TCA concentration.

As defined by equation (3), the number of Ag-coated PMMA particles increases, the contact resistance of TCA drops down because the particles are connected in parallel. However, as shown in Figure 2c, the resistance does not decrease significantly with concentration. The reason can be explained by the increasing factor. As the concentration of TCA increases, the probability that all conductive particles will not be uniformly contacted increases. When the concentration of TCA is more than 0.5 wt%, the dispersed conductive particles are gradually accumulated together, and if the conductive particles are concentrated to 50 wt%, the conductive particles cover the area with the hexagonal shape (Figure 10). At the large concentration of TCA over 0.5wt%, there is the decrease of contact area for each particle[36]. Therefore, the constriction resistance of each particle in TCA increases. As a result, because TCA layer with high concentration over 0.5wt% does not significantly reduce the resistance and greatly deteriorates the transmittance, it is not suitable for tandem devices. On the other hand, at the TCA concentration of 0.5 wt% or less, the transmittances of TCA layer are similarly good while the contact resistance is somewhat higher. However, the variation of the contact resistance is large at the concentration of 0.005 wt% and 0.05 wt%. It can be elucidated by that there is a large variation in the number of conductive particles within a fixed contact area of 0.25cm^2, shown in Figure 11. Resultingly, at 0.5 wt% TCA layer, the conductive particles are dispersed well with good transmittance and its contact resistance is consistently low with $5.46 \times 10^{-2}\ \Omega \cdot cm^2$ of the average resistance. Therefore 0.5wt% TCA is considered to be most suitable. Figure 9b shows the contact resistance of the bonded Ag deposited glass/TCA/Ag deposited planar silicon (or textured silicon) samples with various contact area. Both samples with the planar silicon and samples with the textured silicon have perfect ohmic contacts. On the textured surface, the contact resistance of TCA is somewhat higher than that of the planar surface due to the roughness. However both has sufficiently excellent electrical characteristics as TCA. As the contact area increases, the contact resistance increases for both samples. However, in common sense, the contact resistance is a unit independent of the contact area and the value should not be changed with increasing contact area. This increase can be explained by the fact that as the contact

area increases, the conductive particles are dispersed non-uniformly or agglomerated to increase the contact resistance. Nevertheless, even on the 1 cm^2 area sample, the contact resistance of TCA is still very low, less than 0.2 $\Omega \cdot cm^2$. It was demonstrated that our TCA works well as transparent adhesives and electrical connection even on the textured surface and large area without any significant loss.

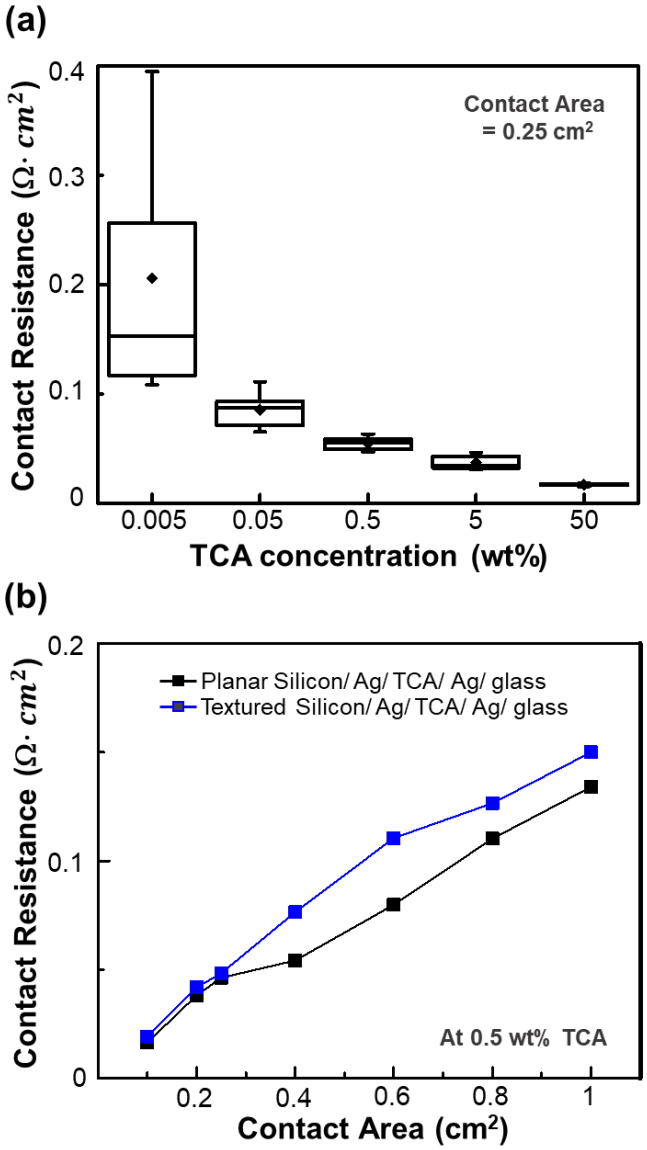

Figure 9. (a) The contact resistance of the TCA layer as function of the concentration of TCA. The contact area is 0.25cm^2. (b) The contact resistance of Ag-deposited glass/TCA/Ag-deposited planar silicon (black line) and Ag-deposited glass/TCA/Ag-deposited textured silicon (blue line) with varying contact area.

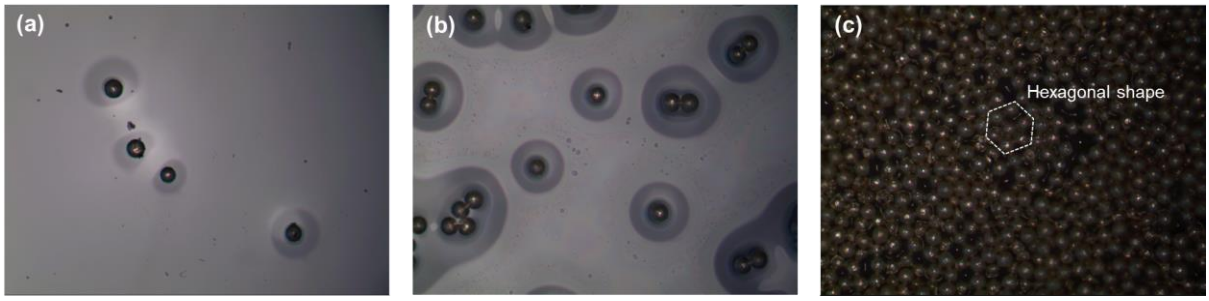

Figure 10. The optical microscope images of (a) 0.5 wt% TCA layer on glass, (b) 5 wt% TCA layer on glass and (c) 50 wt% TCA layer on glass.

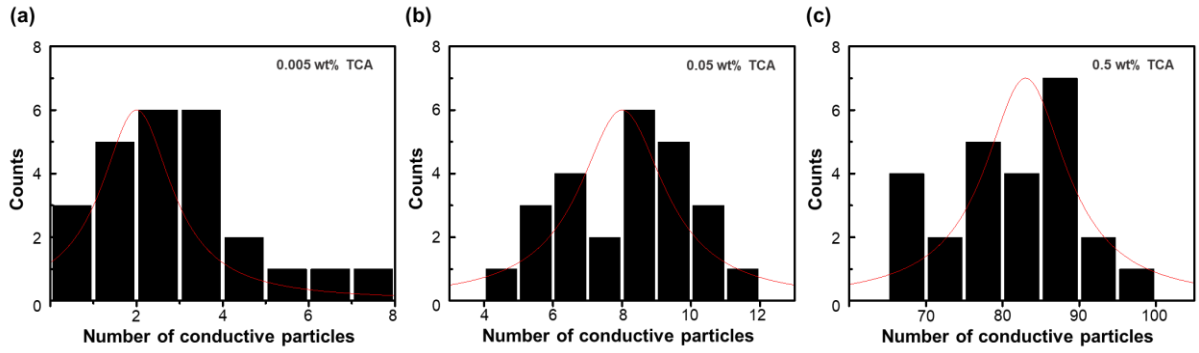

Figure 11. Histograms of the number of conductive particles (Ag-coated PMMA particles) on (a) 0.005 wt% TCA layer, (b) 0.05 wt% TCA layer and (c) 0.5 wt% TCA layer. These are measured for 30 individual samples with fixed area of 0.25cm^2.

4-2. Optical Simulation for the highest current density

For the 2-terminal tandem device where two sub cells are connected in series, the current matching is crucial point because the current density is determined by the lower one between that of two cells. When measuring the current of the silicon bottom cell by filtering the ST perovskite top cell with normal thickness, the current of the silicon bottom cell was much smaller than the current of the perovskite top cell. In our devices, the current density is highly limited by the silicon bottom cells. Therefore, before directly fabricating the tandem devices, we considered the optimal conditions to enhance the current density of the silicon bottom cell through optical simulations using the refractive index, *n* and the extinction coefficient, *k* values of each layer. The refractive indices of each layer were measured by ellipsometry. Figure 12 depicts the refractive index profile of all layers for perovskite/silicon tandem device. For the typical silicon solar cells, 70-80 nm thick SiN_x layer with a refractive index of 1.97 is usually used because it has the lowest reflectance at 550 nm of wavelength where has the most high intensity of the solar spectrum[37]. However, in case of the silicon bottom cell for the tandem device, the infrared region from 800 nm to 1100 nm is the region where the silicon bottom cell mostly absorbs because the perovskite top cell with 1.55 eV of bandgap absorbs the most of the short-wavelength light. To minimize the reflectance and enhance the light absorption, 30nm thick IZO which has similar refractive index of 1.83 was used on the 70nm thick SiN_x layer and the double layers on silicon has lower reflectance especially for the infrared region than only 70 nm thick SiN_x layer on silicon as shown in Figure 13.

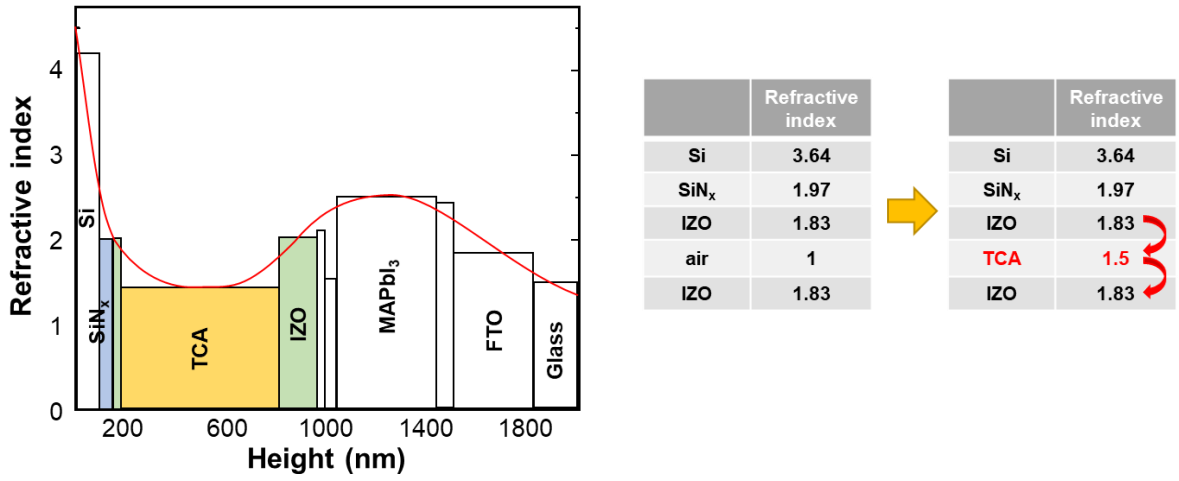

Figure 12. Refractive index profile of each layer of the 2-terminal mechanical silicon/perovskite tandem devices.

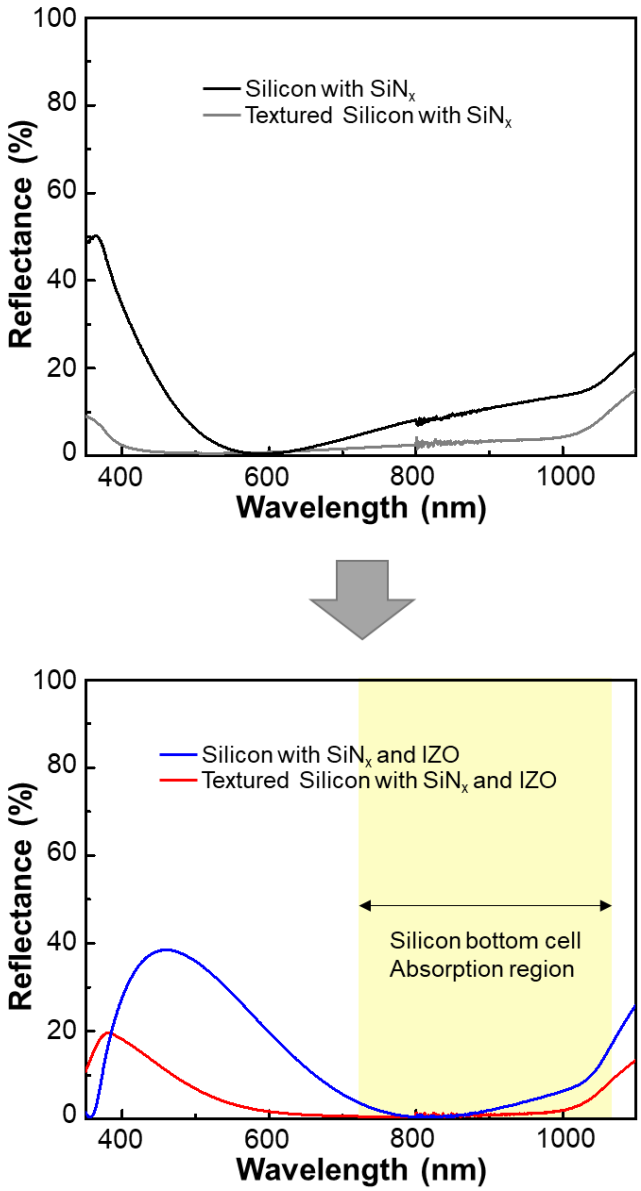

Figure 13. The reflectance spectra of the silicon solar cells with only SiN_x 70nm (black line with planar silicon and gray line with textured silicon) and with SiN_x 70nm and IZO 30nm (blue line with planar silicon and red line with textured silicon).

As a result, the reflectance of tandem device was reduced from 6.95 mA/cm^2 without the IZO layer to 5.52mA/cm^2 with optimal thickness of IZO layer and the absorption and the simulated maximum current density of silicon bottom cells which are filtered by top cell increased to 10.58 mA/cm^2 with IZO/SiN_x double layer from 10.24 mA/cm^2 with only SiN_x layer. A 45 um thick TCA layer between two sub-cells makes the refractive index profile smooth from 1.83 of IZO to 1.56 of TCA to 1.83 of IZO which is better than from 1.83 of IZO to 1 of Air to 1.83 of IZO, as shown in Figure 3a. It makes to reduce the reflection losses of the tandem device from 6.39 mA/cm^2 to 5.52 mA/cm^2 (Figure 14a) and then extract more light from the perovskite top cells especially at the infrared region without any decrease in absorption of perovskite top cells (Figure 14b).

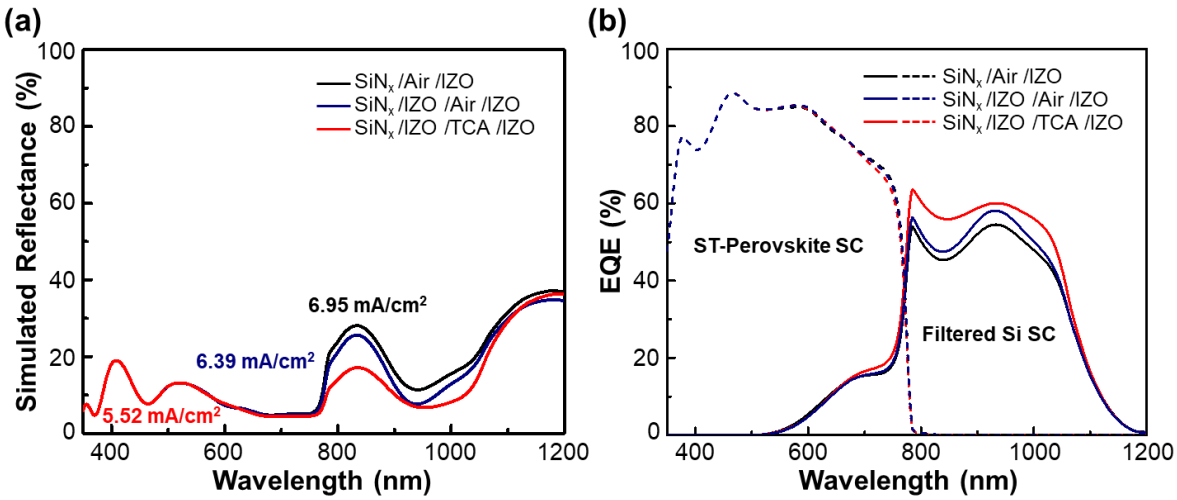

Figure 14. (a) Simulated reflectance of the mechanical tandem devices and (b) simulated external quantum efficiency (EQE) of the perovskite top cells and filtered silicon bottom cells for optimal device design.

Although there is quite enhancement of the absorption for the silicon bottom cells through the refractive index matching, the silicon bottom cells have the low current density compared to the perovskite top cells. For balancing of the light absorption and matching the current density of the perovskite top cells and the silicon bottom cells, methods of tuning the band gap of the perovskite layer or adjusting the thickness of the perovskite layer are possible. Of the two methods, we chose the latter and calculated the maximum current density of each sub cells as function of the thickness of perovskite absorbing layer[38, 39]. The current density of the perovskite top cells and the silicon bottom cells has the trade-off relationship with the thickness of perovskite layer. Figure 15a shows the simulated absorption spectra of the two sub cells with different thickness of perovskite layer. As the perovskite thickness decreases, the absorption of the perovskite top cells gradually decreases and the absorption of the silicon bottom cells increases especially at the wavelength of 400-800 nm. Figure 15b shows the simulated maximum current density of each cell with the different thickness of the perovskite layer. We used the gold electrode for the opaque perovskite solar cells (black line) and the IZO electrode for the semi-transparent perovskite solar cells which are the top cell for the tandem devices (gray line). As thickness of perovskite layer increases, the current density of both the opaque and the semi-transparent perovskite solar cells decrease. The maximum current density of silicon solar cells with IZO thin layer gradually increased with decreasing the thickness of the perovskite layer (blue line)[21]. With TCA, there is quite more enhancement (red line) as we expected above. The current density of the perovskite top cells and the silicon bottom cells has the trade-off relationship. The maximum current densities of the two sub cells are matched at the 150 nm thick perovskite layer and the calculated maximum current density of the tandem device is 14.95 mA/cm^2.

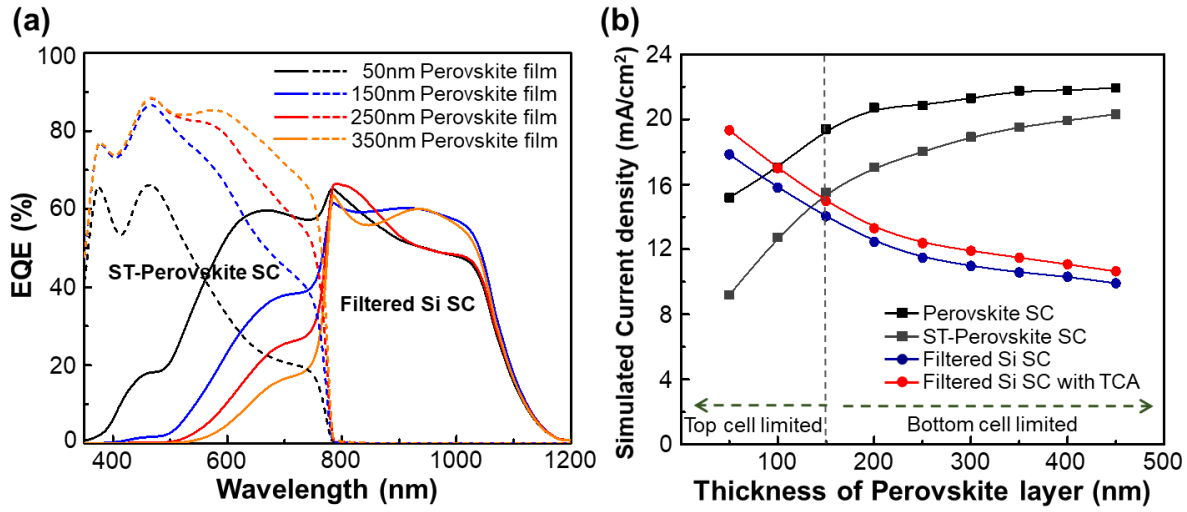

Figure 15. Simulated (a) EQE and (b) maximum current density of each sub-cell by changing the thickness of the $MAPbI_3$ perovskite film.

Figure 16 demonstrate the simulated reflectance and absorption of each layer of tandem devices with the 150 nm thick perovskite layer. The calculated current losses and gains of each layer is summarized in Table 2. Although the region where silicon can absorb is quite limited due to the high parasitic absorption of the glass, FTO and IZO layers especially at long wavelength region, by reducing the thickness of the perovskite layer to 150 nm, it absorbed more light in the wavelength of 600-800 nm and the absorption of two sub cells maintain a good balance.

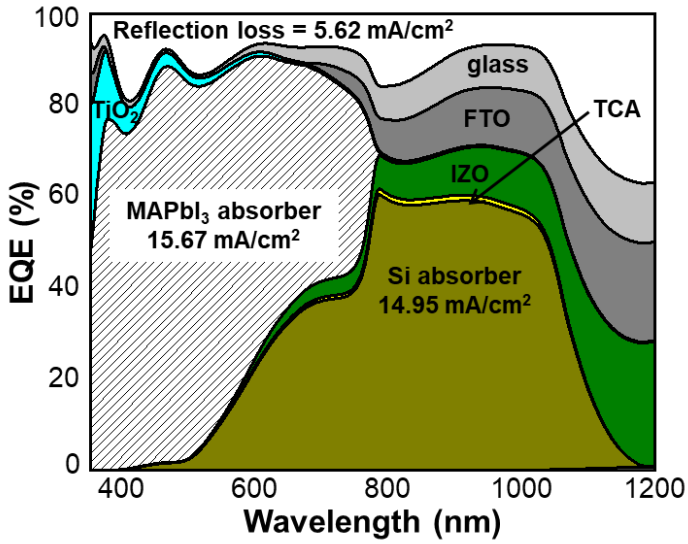

Figure 16. Simulated absorption of each layer in the mechanical tandem devices.

Table 2. Breakdown of optical losses for each layer in the 2-terminal mechanical tandem devices.

Layers	Thickness (μm)	J_{loss} (mA/cm^2)
Reflection		5.62
Glass	18000	2.66
FTO	0.3	3.06
TiO_2	0.07	0.55
$MAPbI_3$	0.15	15.67
PTAA	0.06	0
MoO_3	0.01	0.02
IZO	0.15	2.60
TCA	450	0.31
IZO	0.03	0.61
SiN_x	0.07	0
Si	525	14.95
Ag	2	0.03

4-3. Current matching by controlling thickness of the perovskite

Based on the predicted results from the simulation, the devices were fabricated to confirm that it was also consistent with the experiment. Figure 17 shows the experimental photovoltaic properties of each sub cells with the different thickness of perovskite layer. To balance the absorption and match the current of the tandem devices, we controlled the thickness of the perovskite layer by using the different concentration of the $MAPbI_3$ solutions. The photographs of FTO/bl-TiO_2/mp-TiO_2/$MAPbI_3$ with different concentration of 0.15M, 0.3M, 0.6M, 0.9M, 1.2M and 1.5M were in Figure 17a. The $MAPbI_3$ film was fabricated by one-step process with anti-solvent dropping. It has optical band gap of 1.53 eV (Figure 18a). Each solutions with different concentration generate different thickness of $MAPbI_3$ layer; 50 nm from 0.15M $MAPbI_3$ solutions, 100 nm from 0.3M, 150 nm from 0.6M, 250 nm from 0.9M, 350 nm from 1.2M, and 400 nm from 1.5M, respectively. The thickness of $MAPbI_3$ layers were measured by α-step thickness measurement and SEM analysis. The absorbance of the perovskite film gradually decreased especially at the wavelength of 400-800 nm increased as decreasing the perovskite thickness[40] (Figure 17b). Because the absorbance of the perovskite film reduced with the lower concentration solution of $MAPbI_3$, the current density of the perovskite top cells decreased as you can see *J-V* curve in Figure 17c. The devices with 400 nm, 350 nm, 250 nm and 150 nm of perovskite layer represented the similar open-circuit voltage (*V*oc) and Fill Factor (*FF*). However, the devices with thin perovskite layer like 100 nm and 50 nm had the lower *V*oc than the other thick ones because it is hard to fabricate uniform and compact thin film on the rough FTO substrate (~30 nm RMS) as you can see in Figure 19. In case of the thick film above 150 nm, the uniform and pinhole-free film was fabricated. On the other hand, the thin film below 150 nm had some pinholes which make the leakage current. The summary of the *J-V* characteristics of perovskite solar cells is in the Table 3. To experimentally predict the current density of the tandem devices, the *J-V* curves of the silicon bottom cells were measured in condition of the light filtered by the perovskite top cells.

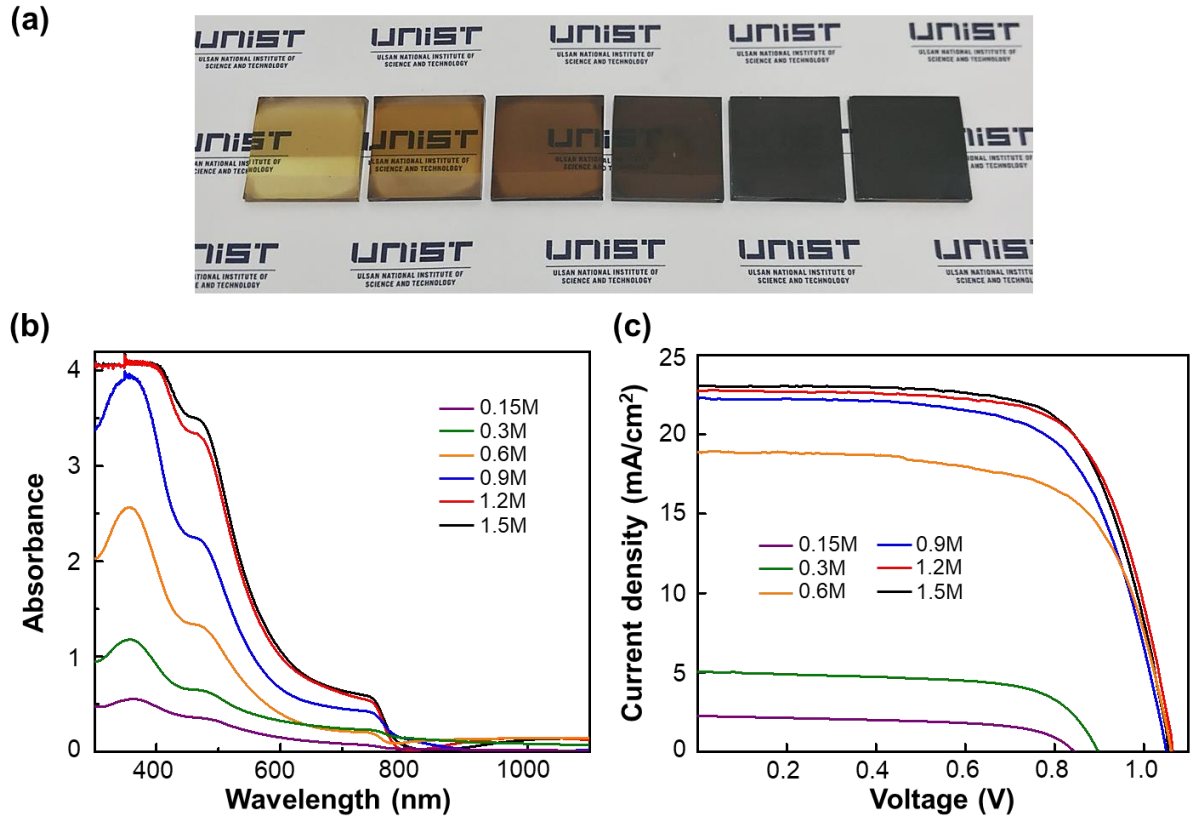

Figure 17. (a) Photographs and (b) Absorbance of glass/FTO/bl-TiO_2/mp-TiO_2/$MAPbI_3$. (c) J-V curves of the opaque perovskite solar cells with different concentration of the $MAPbI_3$ solution.

Table 3. *J-V* characteristics of the opaque perovskite solar cells with different concentration of perovskite solution.

Concentration of perovskite solution	*Jsc* [mA cm^{-2}]	*Voc* [V]	*FF*	*PCE* [%]
1.5M	23.07	1.06	0.70	17.11
1.2M	22.75	1.05	0.70	16.86
0.9M	22.27	1.06	0.68	16.05
0.6M	18.88	1.07	0.66	13.39
0.3M	5.07	0.90	0.65	2.97
0.15M	2.27	0.85	0.59	1.14

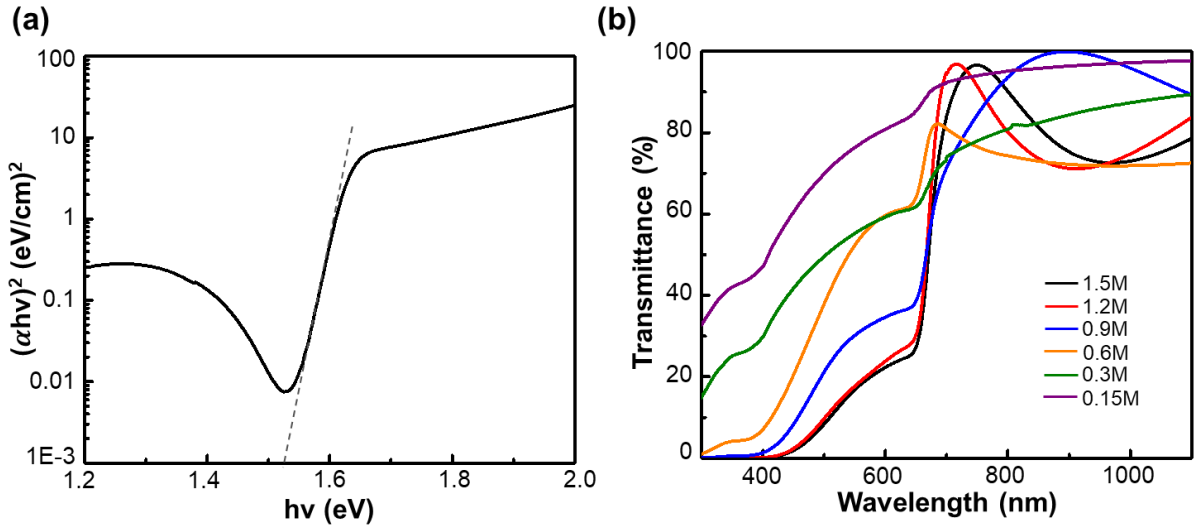

Figure 18. (a) Tauc plot of $MAPbI_3$ perovskite layer and (b) Transmittance of the perovskite layer with different concentration solution.

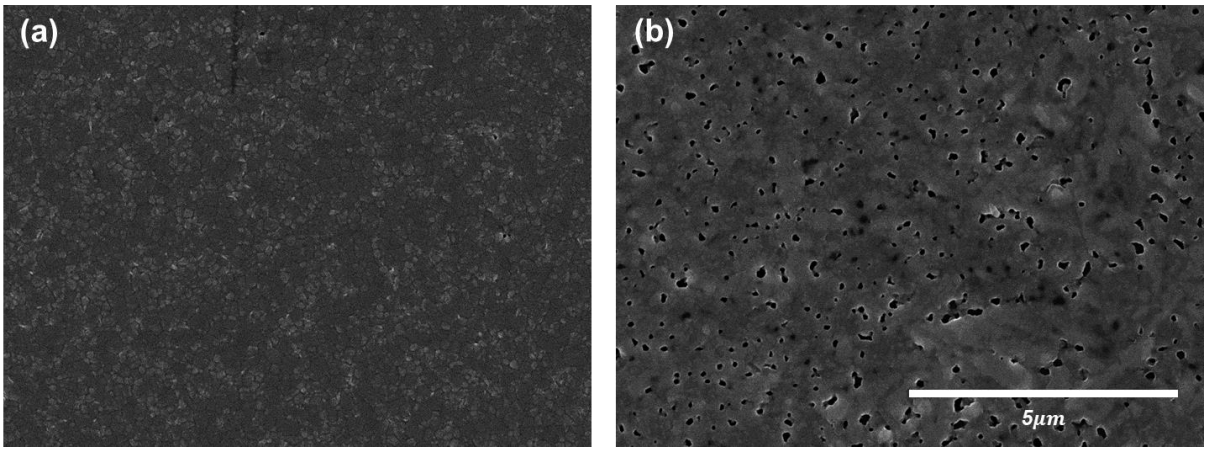

Figure 19. The top view of SEM images of (a) 350nm thick and (b) 100nm thick perovskite layer.

Figure 20a reveals that the current density of the filtered silicon bottom cells gradually increased as the thickness of the perovskite film decreases due to the enhancement of the transmittance of the perovskite film. The average transmittances of 400-800nm wavelength are 38.2% for 1.5M sample, 39.2% for 1.2M sample, 42.2% for 0.9M, 54.5% for 0.6M, 59.5% for 0.3M and 79.0% for 0.15M. (Figure 18b). As we expected with optical simulation, with the trade-off relationship of semi-transparent perovskite solar cells (gray line) and silicon solar cells (blue line), the current of the tandem device was matched at the 150 nm thick perovskite film which from 0.6M $MAPbI_3$ solution. (Figure 20b) The matched current density is 14.80 mA/cm^2.

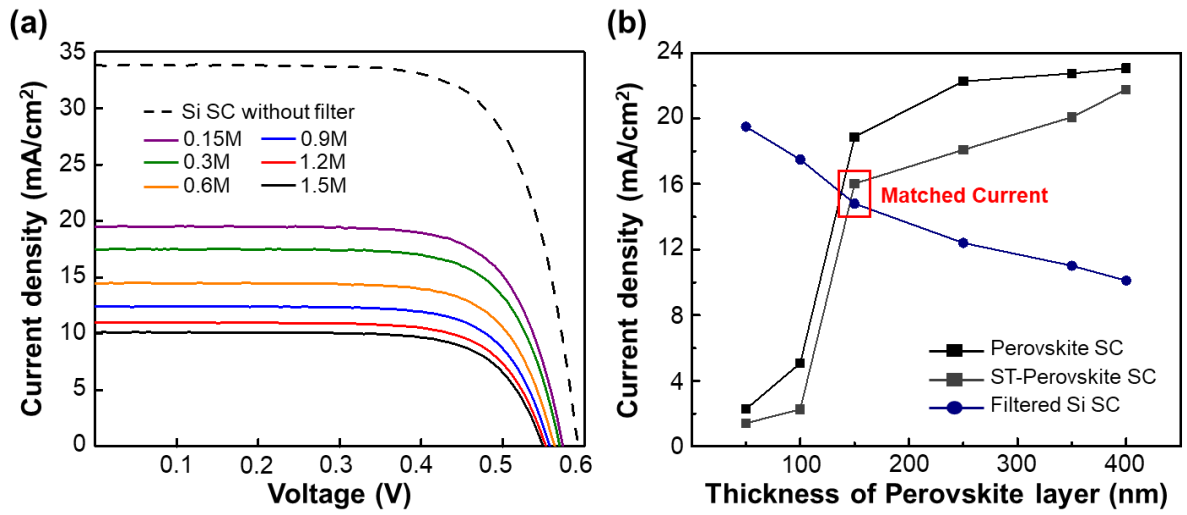

Figure 20. (a) *J-V* curves of silicon solar cell and filtered silicon solar cells with different concentration of the $MAPbI_3$ solution. (b) Experimental current density of each sub cell with different thickness of the perovskite layer. The matched current density is 14.80mA/cm^2 at the 150nm thick perovskite layer.

4-4. Performance of 2-terminal mechanical tandem devices

Compared to the monolithic tandem devices, our mechanical tandem devices perform almost the same characteristics as previously predicted. Figure 21 is the photograph of the real tandem devices. The upper part is the perovskite top cell from glass to IZO layer and the lower part is the silicon bottom cell. They are electrically and mechanically connected with 0.5 wt% TCA in the middle and form a complete one body. The exact active area is 0.25 cm^2. Our tandem device with TCA were cured and bonded strongly, the two sub-cells never detach even with strong force.

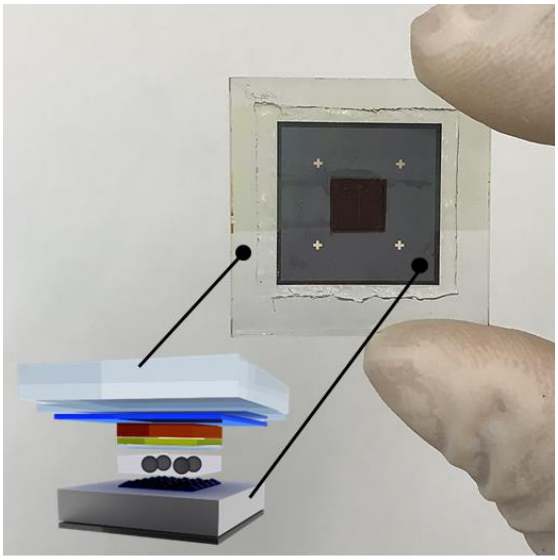

Figure 21. Photograph of a fabricated 2-terminal mechanical perovskite/silicon tandem device.

To evaluate the 4-terminal tandem characteristics, the performance of each sub cell was measured independently. Figure 22 shows *J-V* curves of the 4-terminal perovskite/silicon tandem devices with 150 nm thick $MAPbI_3$ film. Without filter, the planar silicon solar cells preformed 33.87 mA/cm^2 of the current density and 14.81% of efficiency. With the perovskite filter with 150 nm thick $MAPbI_3$ film, the filtered silicon solar cell with 150nm thick $MAPbI_3$ has 14.48 mA/cm^2 of the current density, 6.47% of the efficiency. Compared to the planar silicon solar cells, the textured silicon solar cells have boosted the current density due to the enhanced light absorption[41]. In case of semi-transparent perovskite solar cells with 150 nm thick $MAPbI_3$, it performed average 10.36% efficiency with 16.05 mA/cm^2 of the current density and 1.02V of *V*oc on reverse scan. As a results, the efficiency of 4-terminal tandem devices was 16.73% for planar silicon/perovskite and 17.15% for textured silicon/perovskite.

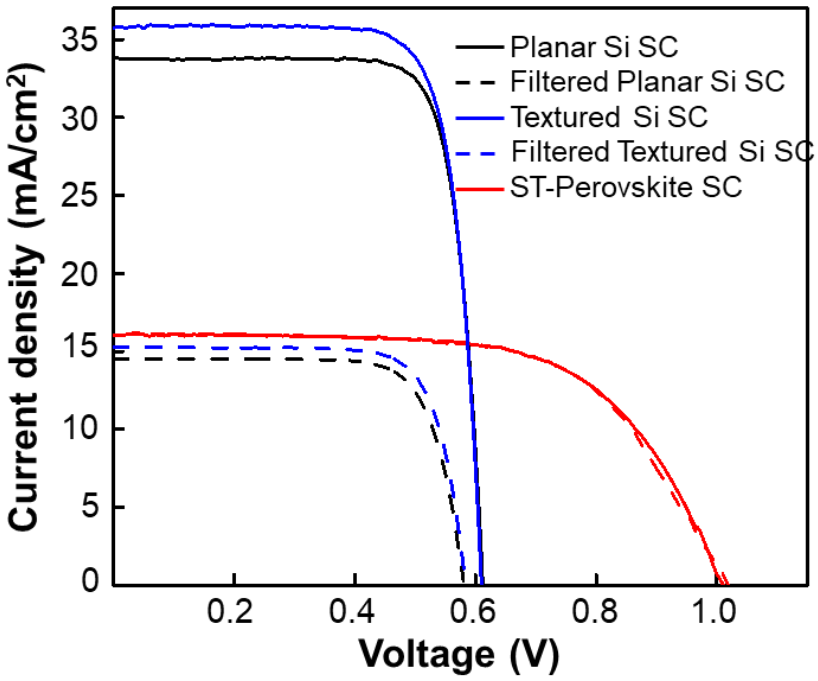

Figure 22. *J-V* curve of the 4-terminal mechanical tandem devices with planar silicon solar cells (black line) and with textured silicon solar cells (blue line).

The *J-V* curves of the optimized 2-terminal mechanical perovskite/silicon tandem devices with TCA were presented in Figure 23. The 17.47% of efficiency for tandem devices based on planar silicon cells and perovskite cells with 150nm thick perovskite layer is achieved with a 14.36 mA/cm^2 of the *J*sc, 1.58 V of *V*oc, 0.77 of *FF* under reverse scan. The current density is well matched as we expected from the current density of the filtered silicon solar cell. Also, the loss of *V*oc is just below 2% due to the low contact resistance of the TCA layer. Without the lateral charge transporting, the electron charges are vertically transported.

As described in Figure 24, when we fabricated the tandem devices with a perovskite solar cells having various thickness by various concentration of $MAPbI_3$ solution, it is confirmed that the tandem devices fabricated with the 0.6M $MAPbI_3$ solution had the highest current density and the highest efficiency. It is very consistent with the results expected in the previous figure.

Figure 25 shows the performance of the tandem devices by concentration of TCA. At the TCA concentration of 0.5 wt% or less, the tandem devices performed the similar current density of 14.3 mA/cm^2. However, as the TCA concentration decreases, FF value is reduced with increasing the series resistance (R_s). It is influenced by the contact resistance of TCA layer. When 5 wt% TCA is used, it has the lower transmittance than others, while the series resistance is the lowest, so the current density was reduced accordingly. As a result, the best performance was obtained when using 0.5 wt% TCA. When it is applied to textured silicon cell, the TCA electrically and mechanically connects the two sub cell well even on the textured surface. As a result, Perovskite/the textured Si tandem device has the increased current density of 15.10 mA/cm^2 due to the enhanced light absorption and 18.33% of efficiency is achieved. The *J-V* characteristics of tandem devices are summarized in the Table 3.

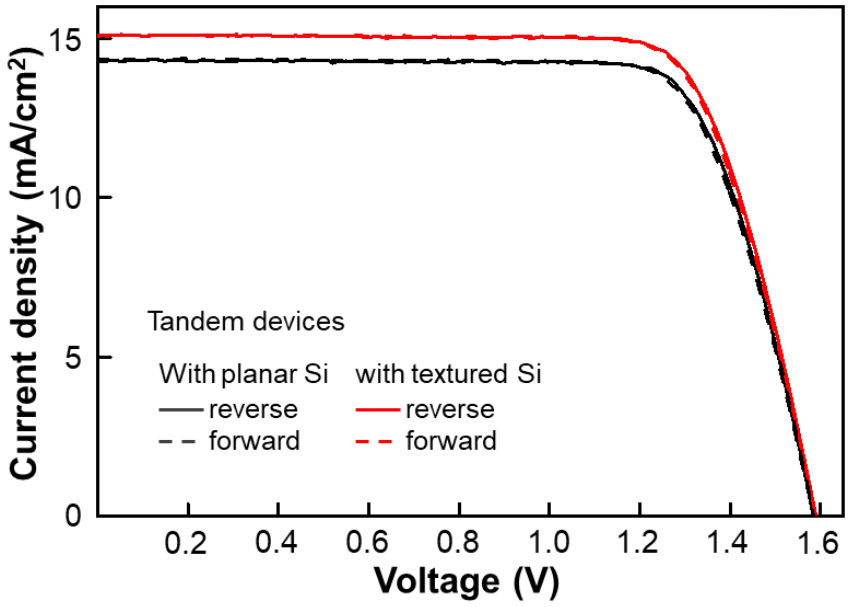

Figure 23. *J-V* curve of the 2-terminal mechanical tandem devices with planar silicon solar cells (black line) and with textured silicon solar cells (red line). Full line reveals the reverse scan and dash line reveals the forward scan.

Table 4. *J-V* characteristics of the tandem devices.

		Jsc [mA cm^{-2}]	*Voc* [V]	*FF*	*PCE* [%]
Al-BSF planar Si solar cell	(without filter)	33.86	0.61	0.79	16.32
	(with filter)	14.48	0.58	0.76	6.38
Al-BSF textured Si solar cell	(without filter)	35.73	0.61	0.78	17.00
	(with filter)	15.25	0.58	0.77	6.80
ST-Perovskite solar cell	(reverse scan)	16.05	1.02	0.63	10.36
	(forward scan)	16.04	1.01	0.64	10.34
4-terminal Tandem solar cell (with planar Si/ with textured Si)					16.73/ 17.15
2-terminal Tandem solar cell with planar Si	(reverse scan)	14.32	1.58	0.77	17.42
	(forward scan)	14.36	1.58	0.77	17.47
2-terminal Tandem solar cell with textured Si	(reverse scan)	15.10	1.59	0.76	18.33
	(forward scan)	15.07	1.59	0.76	18.33

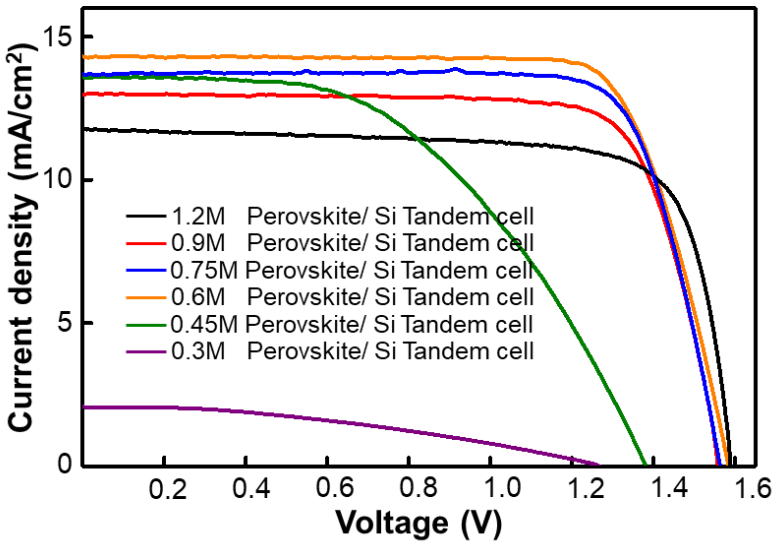

Figure 24. *J-V* characteristics of the 2-terminal mechanical tandem devices with different concentration of perovskite solution. The matched maximum current is achieved at 0.6M perovskite layer.

Table 5. *J-V* characteristics of the 2-terminal mechanical tandem devices with different concentration of perovskite solution.

Concentration of perovskite layer	*Jsc* [mA cm^{-2}]	*Voc* [V]	*FF*	*PCE* [%]
1.2M Perovskite/ Silicon Tandem	11.77	1.59	0.76	14.22
0.9M Perovskite/ Silicon Tandem	12.97	1.56	0.77	15.58
0.75M Perovskite/ Silicon Tandem	13.69	1.47	0.78	16.75
0.6M Perovskite/ Silicon Tandem	14.32	1.58	0.77	17.42
0.45M Perovskite/ Silicon Tandem	13.59	1.38	0.50	9.43
0.3M Perovskite/ Silicon Tandem	2.07	1.28	0.38	1.00

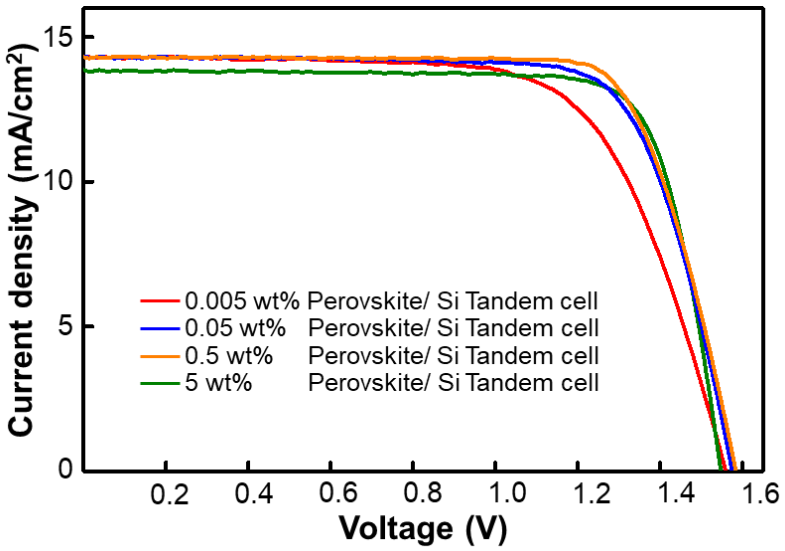

Figure 25. *J-V* characteristics of the 2-terminal mechanical tandem devices with different concentration of TCA.

Table 6. *J-V* characteristics of the 2-terminal mechanical tandem devices with different concentration of TCA.

TCA Concentration [wt%]	*J*sc [mA cm^{-2}]	*V*oc [V]	*FF*	*PCE* [%]	R_s [ohm cm^2]
0.005	14.34	1.56	0.68	15.10	0.016
0.05	14.32	1.58	0.75	16.86	0.011
0.5	14.32	1.58	0.77	17.42	0.011
5	13.87	1.55	0.79	16.98	0.008

In order to further decrease the light reflection from the glass substrate, we integrated an AR foil on top of the glass[21, 42]. Actually, when filtering the silicon solar cell by glass/FTO, there is significant decreasing in light absorption of silicon solar cells as you can see in Figure 26. It is because of the low light transmittance of glass/FTO. As a solution for that, the home-made AR foil which was fabricated by pyramidal textured silicon mold elongates the light path. As shown in Figure 27a, AR foil on the glass looks different depending on the distance from the background due to scattering of light. Therefore, when it is integrated on top of the tandem device, it reduces the average reflectance of the tandem device from 12.26% to 9.35% (Figure 27b).

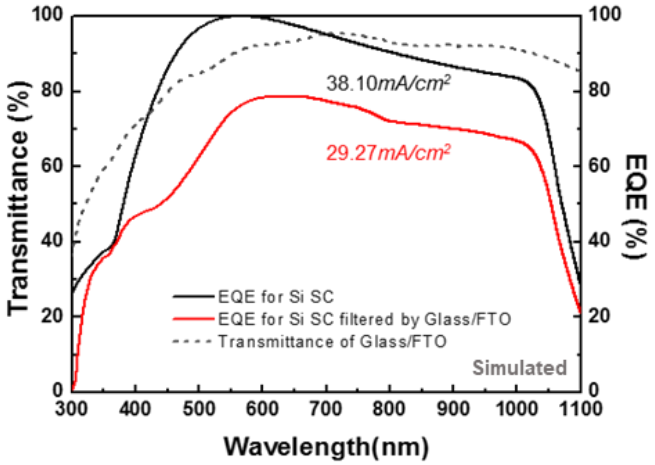

Figure 26. The simulated EQE of silicon solar cell (black line) and filtered silicon solar cell by glass/FTO and the measured transmittance of glass/FTO.

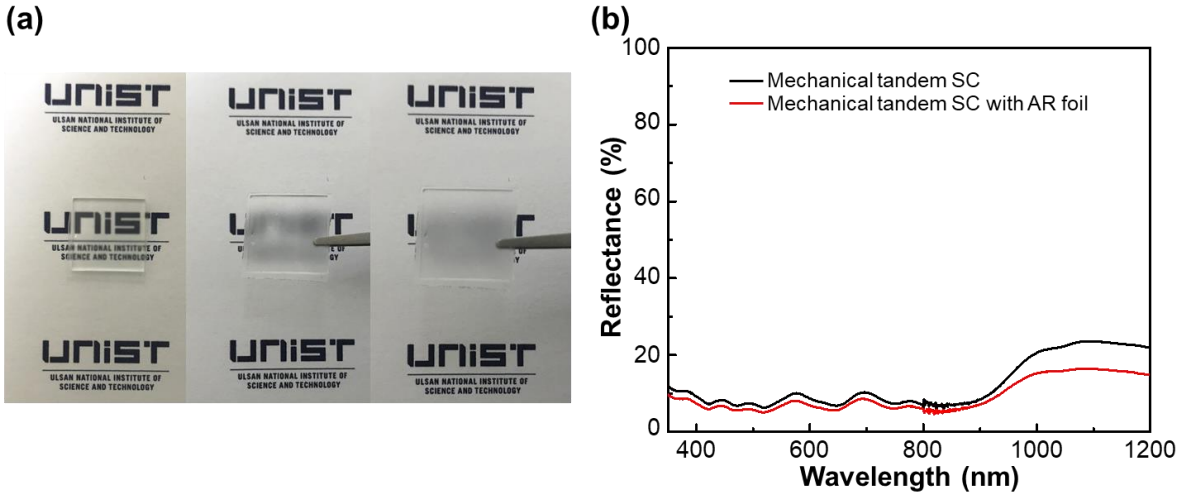

Figure 27. (a) Photographs of home-made AR foil on the glass depending on the distance from the background. (b) Measured reflectance of the final mechanical tandem devices with and without AR foil.

Figure 28 demonstrates that the champion perovskite/the textured silicon tandem devices with AR foil has 15.43 mA/cm^2 of the current density and 19.40% of the steady-state efficiency. This is the highest efficiency in reported 2-terminal mechanical tandem devices. In addition, our tandem devices are stable in humid condition (RH=85% at RT) without the entire encapsulation because the top perovskite cell based on glass is covered the silicon solar cell and the air-unstable perovskite layer is completely sealed by TCA layer. As you can see in Figure 28c, in the 85% humidity condition, our tandem device without additional encapsulation has only small degradation less 10% in efficiency for 100 hours, as a perovskite single cell encapsulated with EVA/glass. Although it is less efficient than reported 2-terminal monolithic tandem structure, it is promising structure when considering the simplicity of fabrication and stability. Especially, it is also excellent on the aspect of commercialization. Compared to monolithic tandem structure which needs new deposition methods of perovskite top cell for use of textured silicon bottom cell, our mechanical tandem structure can use the commercial Al-BSF textured silicon solar cell through just simple TCA coating process without any process change.

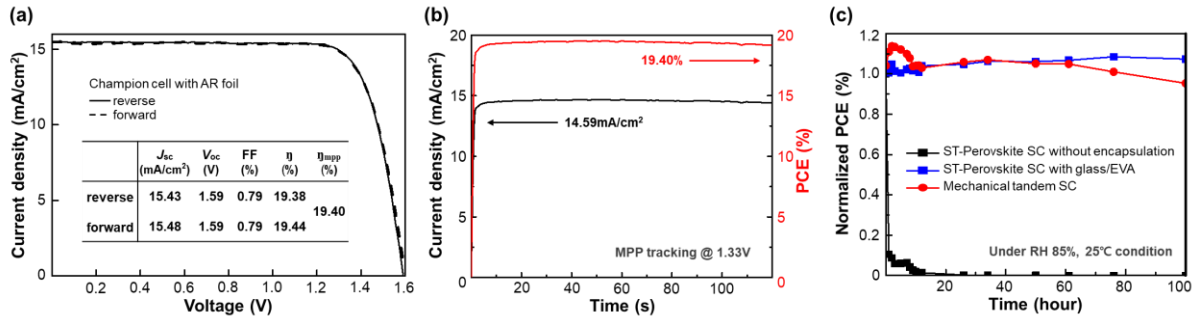

Figure 28. The champion 2-terminal mechanical tandem device performance. (a) *J-V* curve and (b) steady-state PCE of our champion 2-terminal mechanical tandem device based on textured silicon solar cells with AR foil. (c) Normalized efficiency of ST-perovskite solar cell with/without encapsulation and the tandem device for 100 hours in RH 85%, 25℃ condition.

4-5. Future Outlook

In our current tandem structure, there is a large amount of the parasitic absorption in the long wavelength region through the glass, FTO and IZO, and *Voc* is limited because band gap of the perovskite layer is not tuned. There is a room to improve the efficiency of the tandem devices. Higher performance is expected, if the parasitic absorption is minimized, the band gap and thickness of the perovskite layer are tuned appropriately for perovskite top cells and PERC structure is introduced for silicon bottom cells. Silicon solar cell with PERC structure is a low-cost and high-efficiency cells that will lead the solar cell market in near future by replacing the Al-BSF structure. As compared with the Al-BSF structure, well-passivated PERC structure has higher light absorption especially in the long wavelength region and it is very suitable for tandem structure where light absorption in long wavelength region has great effect on the current enhancement as you can see in Figure 29 and Table 7 [43-45].

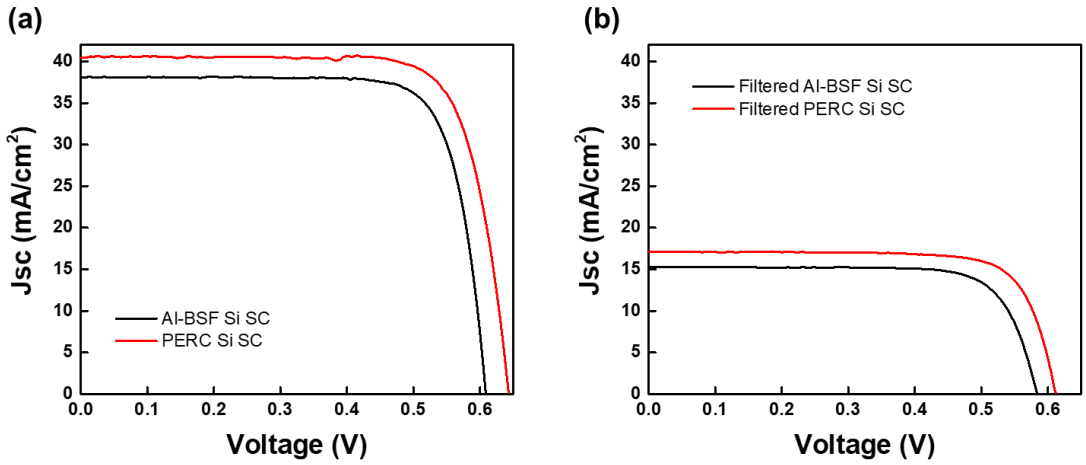

Figure 29. *J-V* characteristics of (a) Al-BSF and PERC silicon solar cells and (b) Al-BSF and PERC silicon solar cells filtered by perovskite top cells.

Table 7. *J-V* characteristics of Al-BSF and PERC silicon solar cells with textured surface.

TCA Concentration [wt%]	*J*sc [mA cm^{-2}]	*V*oc [V]	*FF*	*PCE* [%]
Al-BSF Si SC	38.03	0.61	78	18.15
PERC Si SC	40.45	0.65	77	20.12
Filtered Al-BSF Si SC by perovskite cell	15.25	0.58	77	6.80
Filtered PERC Si SC by perovskite cell	17.10	0.61	77	8.05

Figure 30 represents the simulated results of the maximum current density and efficiency of the 2-terminal mechanical tandem devices obtained by adjusting the band gap and thickness of the perovskite layer. In particular, when the tandem device is fabricated with a 350 nm thick perovskite layer with a 1.6 eV of band gap and the PERC silicon solar cell, the highest current density over 18 mA/cm^2 and the highest efficiency over 24% are expected. If realized, it is anticipated to open a new chapter in the solar cell market.

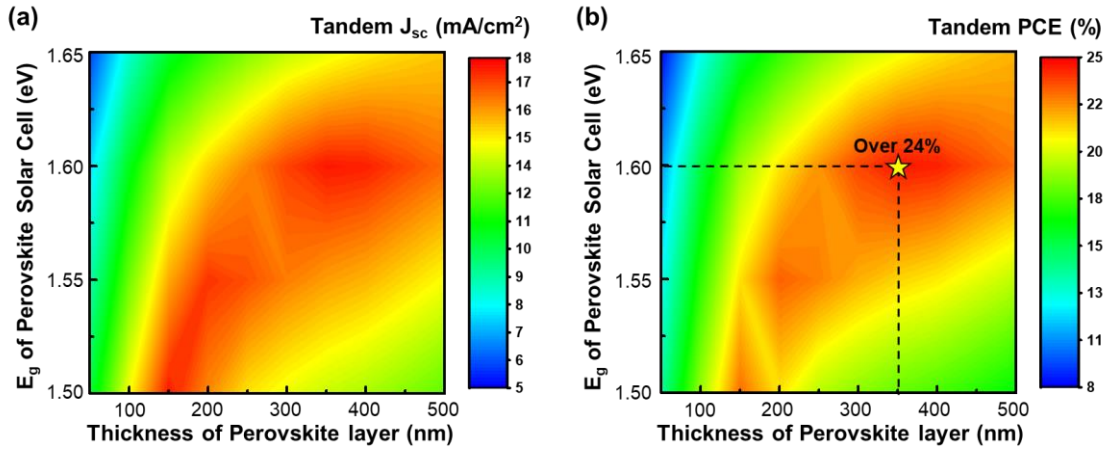

Figure 30. Simulated contour plots of (a) the maximum current density and (b) efficiency of the 2-terminal mechanical tandem devices as function of band gap and thickness of the perovskite layer.

V. Conclusion

In conclusion, we have demonstrated the 19.40% of 2-terminal mechanical perovskite/silicon tandem devices with transparent conductive adhesive by optically controlling the refractive index profile and perovskite absorbing layer thickness. This structure is very promising because it can utilize existing commercialized Al-BSF or PERC silicon solar cells by adding simple TCA solution process. If a high efficiency of over 24% is achieved with the advanced cell design, it is anticipated to open a new chapter in the solar cell market.

VI. References

1. Priscila Gonçalves Vasconcelos Sampaioa, M. O. A. G., Photovoltaic solar energy: Conceptual framework. *Renewable and Sustainable Energy Reviews* **2017,** *74*, 590-601.
2. NREL Best Research-Cell Efficiencies.
3. Armin Richter, M. H., and Stefan W. Glunz, Reassessment of the Limiting Efficiency for Crystalline Silicon Solar Cells. *IEEE Journal of Photovoltaics 2013* **2013**.
4. Werner, J.; Niesen, B.; Ballif, C., Perovskite/Silicon Tandem Solar Cells: Marriage of Convenience or True Love Story? - An Overview. *Advanced Materials Interfaces* **2018,** *5* (1).
5. Bo Chen, X. Z., Yang Bai, Nitin P. Padture, and Jinsong Huang, progress in tandem solar cells based on hybrid organic–inorganic perovskites. *Adv. Energy Mater.* **2017,** *7*.
6. Polman, A.; Atwater, H. A., Photonic design principles for ultrahigh-efficiency photovoltaics. *Nat Mater* **2012,** *11* (3), 174-7.
7. David P. McMeekin, G. S., Waqaas Rehman, Giles E. Eperon, Michael Saliba, Maximilian T. Hörantner, Amir Haghighirad, Nobuya Sakai, Lars Korte, Bernd Rech, Michael B. Johnston, Laura M. Herz, Henry J. Snaith, A mixed-cation lead mixed-halide perovskite absorber for tandem solar cells. *SCIENCE* **2016,** *351*.
8. De Wolf, S.; Holovsky, J.; Moon, S. J.; Loper, P.; Niesen, B.; Ledinsky, M.; Haug, F. J.; Yum, J. H.; Ballif, C., Organometallic Halide Perovskites: Sharp Optical Absorption Edge and Its Relation to Photovoltaic Performance. *J Phys Chem Lett* **2014,** *5* (6), 1035-9.
9. Zhao, Y.; Nardes, A. M.; Zhu, K., Mesoporous perovskite solar cells: material composition, charge-carrier dynamics, and device characteristics. *Faraday Discuss* **2014,** *176*, 301-12.
10. Futscher, M. H.; Ehrler, B., Efficiency Limit of Perovskite/Si Tandem Solar Cells. *ACS Energy Letters* **2016,** *1* (4), 863-868.
11. Yu, Z.; Leilaeioun, M.; Holman, Z., Selecting tandem partners for silicon solar cells. *Nature Energy* **2016,** *1* (11).
12. Sarah R. Kurtz, P. F., and J. M. Olson, Modeling of two-junction, series-connected tandem solar cells using top-cell thickness as an adjustable parameter. *Journal of Applied Physics* **1990,** *68*.
13. Zongqi Li, Y. Z., Xi Wang, Yuchao Sun, Zhiguo Zhao, Yujing Li, Huanping Zhou, and Qi Chen, Cost Analysis of Perovskite Tandem Photovoltaics. *Joule* **2018,** *2*.
14. Fan, R.; Zhou, N.; Zhang, L.; Yang, R.; Meng, Y.; Li, L.; Guo, T.; Chen, Y.; Xu, Z.; Zheng, G.; Huang, Y.; Li, L.; Qin, L.; Qiu, X.; Chen, Q.; Zhou, H., Toward Full Solution Processed Perovskite/Si Monolithic Tandem Solar Device With PCE Exceeding 20%. *Solar RRL* **2017,** *1* (11).
15. Jaysankar, M.; Qiu, W.; van Eerden, M.; Aernouts, T.; Gehlhaar, R.; Debucquoy, M.; Paetzold, U. W.; Poortmans, J., Four-Terminal Perovskite/Silicon Multijunction Solar Modules. *Advanced Energy Materials* **2017,** *7* (15).
16. Werner, J.; Barraud, L.; Walter, A.; Bräuninger, M.; Sahli, F.; Sacchetto, D.; Tétreault, N.; Paviet-Salomon, B.; Moon, S.-J.; Allebé, C.; Despeisse, M.; Nicolay, S.; De Wolf, S.;

Niesen, B.; Ballif, C., Efficient Near-Infrared-Transparent Perovskite Solar Cells Enabling Direct Comparison of 4-Terminal and Monolithic Perovskite/Silicon Tandem Cells. *ACS Energy Letters* **2016,** *1* (2), 474-480.

17. Bush, K. A.; Palmstrom, A. F.; Yu, Z. J.; Boccard, M.; Cheacharoen, R.; Mailoa, J. P.; McMeekin, D. P.; Hoye, R. L. Z.; Bailie, C. D.; Leijtens, T.; Peters, I. M.; Minichetti, M. C.; Rolston, N.; Prasanna, R.; Sofia, S.; Harwood, D.; Ma, W.; Moghadam, F.; Snaith, H. J.; Buonassisi, T.; Holman, Z. C.; Bent, S. F.; McGehee, M. D., 23.6%-efficient monolithic perovskite/silicon tandem solar cells with improved stability. *Nature Energy* **2017,** *2* (4).

18. Sahli, F.; Kamino, B. A.; Werner, J.; Bräuninger, M.; Paviet-Salomon, B.; Barraud, L.; Monnard, R.; Seif, J. P.; Tomasi, A.; Jeangros, Q.; Hessler-Wyser, A.; De Wolf, S.; Despeisse, M.; Nicolay, S.; Niesen, B.; Ballif, C., Improved Optics in Monolithic Perovskite/Silicon Tandem Solar Cells with a Nanocrystalline Silicon Recombination Junction. *Advanced Energy Materials* **2018,** *8* (6).

19. Bush, K. A.; Manzoor, S.; Frohna, K.; Yu, Z. J.; Raiford, J. A.; Palmstrom, A. F.; Wang, H.-P.; Prasanna, R.; Bent, S. F.; Holman, Z. C.; McGehee, M. D., Minimizing Current and Voltage Losses to Reach 25% Efficient Monolithic Two-Terminal Perovskite–Silicon Tandem Solar Cells. *ACS Energy Letters* **2018,** *3* (9), 2173-2180.

20. Sahli, F.; Werner, J.; Kamino, B. A.; Brauninger, M.; Monnard, R.; Paviet-Salomon, B.; Barraud, L.; Ding, L.; Diaz Leon, J. J.; Sacchetto, D.; Cattaneo, G.; Despeisse, M.; Boccard, M.; Nicolay, S.; Jeangros, Q.; Niesen, B.; Ballif, C., Fully textured monolithic perovskite/silicon tandem solar cells with 25.2% power conversion efficiency. *Nat Mater* **2018,** *17* (9), 820-826.

21. Zheng, J.; Lau, C. F. J.; Mehrvarz, H.; Ma, F.-J.; Jiang, Y.; Deng, X.; Soeriyadi, A.; Kim, J.; Zhang, M.; Hu, L.; Cui, X.; Lee, D. S.; Bing, J.; Cho, Y.; Chen, C.; Green, M. A.; Huang, S.; Ho-Baillie, A. W. Y., Large area efficient interface layer free monolithic perovskite/homo-junction-silicon tandem solar cell with over 20% efficiency. *Energy & Environmental Science* **2018,** *11* (9), 2432-2443.

22. Green, M. A., Lambertian light trapping in textured solar cells and light-emitting diodes: analytical solutions. *Progress in Photovoltaics: Research and Applications* **2002,** *10* (4), 235-241.

23. He, J.; Gao, P.; Yang, Z.; Yu, J.; Yu, W.; Zhang, Y.; Sheng, J.; Ye, J.; Amine, J. C.; Cui, Y., Silicon/Organic Hybrid Solar Cells with 16.2% Efficiency and Improved Stability by Formation of Conformal Heterojunction Coating and Moisture-Resistant Capping Layer. *Adv Mater* **2017,** *29* (15).

24. Kanda, H.; Uzum, A.; Nishino, H.; Umeyama, T.; Imahori, H.; Ishikawa, Y.; Uraoka, Y.; Ito, S., Interface Optoelectronics Engineering for Mechanically Stacked Tandem Solar Cells Based on Perovskite and Silicon. *ACS Appl Mater Interfaces* **2016,** *8* (49), 33553-33561.

25. Kanda, H.; Shibayama, N.; Uzum, A.; Umeyama, T.; Imahori, H.; Chiang, Y.-H.; Chen, P.; Nazeeruddin, M. K.; Ito, S., Facile fabrication method of small-sized crystal silicon solar cells for

ubiquitous applications and tandem device with perovskite solar cells. *Materials Today Energy* **2018,** *7*, 190-198.

26. C´esar Omar Ram´ırez Quiroz, Y. S., Michael Salvador, Karen Forberich, Nadine Schrenker, George D. Spyropoulos, Thomas Heum¨uller, Benjamin Wilkinson, Thomas Kirchartz, Erdmann Spiecker, Pierre J. Verlinden, Xueling Zhang, Martin A. Green, Anita Ho-Baillie and Christoph J. Brabec, Balancing electrical and optical losses for efficient 4-terminal Si–perovskite solar cells with solution processed percolation electrodes. *Journal of Materials Chemistry A* **2018,** *6*.

27. Henry, C. H., Limiting efficiencies of ideal single and multiple energy gap terrestrial solar cells. *Journal of Applied Physics* **1980,** *51*.

28. Fu, F.; Feurer, T.; Jager, T.; Avancini, E.; Bissig, B.; Yoon, S.; Buecheler, S.; Tiwari, A. N., Low-temperature-processed efficient semi-transparent planar perovskite solar cells for bifacial and tandem applications. *Nat Commun* **2015,** *6*, 8932.

29. Tung, V. C.; Kim, J.; Cote, L. J.; Huang, J., Sticky interconnect for solution-processed tandem solar cells. *J Am Chem Soc* **2011,** *133* (24), 9262-5.

30. Zhang, Y.; Wu, Z.; Li, P.; Ono, L. K.; Qi, Y.; Zhou, J.; Shen, H.; Surya, C.; Zheng, Z., Fully Solution-Processed TCO-Free Semitransparent Perovskite Solar Cells for Tandem and Flexible Applications. *Advanced Energy Materials* **2018,** *8* (1).

31. Shi Wun Tong , Y. W., Yi Zheng , Man-Fai Ng , and Kian Ping Loh, Graphene Intermediate Layer in Tandem Organic Photovoltaic Cells. *Advanced Functional Materials* **2011,** *21*.

32. Yu Bi, S. P., Mehmet Zafer Akgul, Shuchi Gupta, Alexandros Stavrinadis, Jianjun Wang, and Gerasimos Konstantatos, Colloidal Quantum Dot Tandem Solar Cells Using Chemical Vapor Deposited Graphene as an Atomically Thin Intermediate Recombination Layer. *ACS Energy Letters* **2018,** *3*.

33. Talysa R. Klein, B. G. L., Manuel Schnabel, Emily L. Warren, Paul Stradins, Adele C. Tamboli, and Maikel F. A. M. van Hest, Transparent Conductive Adhesives for Tandem Solar Cells Using Polymer−Particle Composites. *ACS Appl. Mater. Interfaces* **2018,** *10*.

34. Sang Hyeon Kim, D.-M. G., Min-Su Park, Chang Zoo Kim, Won Jun Choi, GaAs solar cell on Si substrate with good ohmic GaAs/Si interface by direct wafer bonding. *Solar Energy Materials & Solar Cells* **2015,** *141*.

35. Myung-Jin Yim, S. M., IEEE, and Kyung-Wook Paik, Member, IEEE, Design and Understanding of Anisotropic Conductive Films (ACF's) for LCD Packaging. *IEEE TRANSACTIONS ON COMPONENTS, PACKAGING, AND MANUFACTURING TECHNOLOGY—PART A* **1998,** *21*.

36. Chin, M.; Iyer, K. A.; Hu, S. J., Prediction of Electrical Contact Resistance for Anisotropic Conductive Adhesive Assemblies. *IEEE Transactions on Components and Packaging Technologies* **2004,** *27* (2), 317-326.

37. Duttagupta, S.; Ma, F.; Hoex, B.; Mueller, T.; Aberle, A. G., Optimised Antireflection Coatings using Silicon Nitride on Textured Silicon Surfaces based on Measurements and Multidimensional Modelling. *Energy Procedia* **2012,** *15*, 78-83.

38. Almansouri, I.; Ho-Baillie, A.; Green, M. A., Ultimate efficiency limit of single-junction perovskite and dual-junction perovskite/silicon two-terminal devices. *Japanese Journal of Applied Physics* **2015,** *54* (8S1).

39. Santbergen, R.; Mishima, R.; Meguro, T.; Hino, M.; Uzu, H.; Blanker, J.; Yamamoto, K.; Zeman, M., Minimizing optical losses in monolithic perovskite/c-Si tandem solar cells with a flat top cell. *Opt Express* **2016,** *24* (18), A1288-99.

40. Liu, D.; Gangishetty, M. K.; Kelly, T. L., Effect of CH3NH3PbI3thickness on device efficiency in planar heterojunction perovskite solar cells. *J. Mater. Chem. A* **2014,** *2* (46), 19873-19881.

41. Jaysankar, M.; Filipič, M.; Zielinski, B.; Schmager, R.; Song, W.; Qiu, W.; Paetzold, U. W.; Aernouts, T.; Debucquoy, M.; Gehlhaar, R.; Poortmans, J., Perovskite–silicon tandem solar modules with optimised light harvesting. *Energy & Environmental Science* **2018,** *11* (6), 1489-1498.

42. Hwang, I.; Choi, D.; Lee, S.; Seo, J. H.; Kim, K. H.; Yoon, I.; Seo, K., Enhancement of Light Absorption in Photovoltaic Devices using Textured Polydimethylsiloxane Stickers. *ACS Appl Mater Interfaces* **2017,** *9* (25), 21276-21282.

43. Gatz, S.; Bothe, K.; Müller, J.; Dullweber, T.; Brendel, R., Analysis of local Al-doped back surface fields for high efficiency screen-printed solar cells. *Energy Procedia* **2011,** *8*, 318-323.

44. Green, M. A., The Passivated Emitter and Rear Cell (PERC): From conception to mass production. *Solar Energy Materials and Solar Cells* **2015,** *143*, 190-197.

45. Schmidt, T. D. a. J., Industrial Silicon Solar Cells Applying the Passivated Emitter and Rear Cell (PERC) Concept—A Review. *IEEE Journal of Photovoltaics* **2016,** *3*.

VII. Acknowledgements

First of all, I would like to thank Prof. Kyoung Jin Choi for his guidance and encouragement. During the course of master's degree from undergraduate course, I learned a lot while studying and discussing with you. Also. I would like to thank Prof. Myoung Hoon Song and Prof. Hyesung Park for participating in my depands examination. I am very grateful to meet you and get lots of advice from you.

Thanks to ECO lab members, Chanul, Sungbum, Myeonghoon, Wonjin, Hyungmin, Byungyoon and Dr. Amit, who helped me complete the course for Master's degree for more than three years. I hope that you will have good results in the future. In particular, I am appreciative of 'the solar cell team' members, Chanul, Wonjin and Hyungmin who gave me mental strength and brought me laughter while doing research. I hope all your day is filled with laughter. Also, I would like to express my gratitude to Seyang, Siyoung, Soomin and Chanul (Members of Kkehet) who congratulated me on the good work and comforted me with the sad work always. I hope everyone will graduate soon and take a more wonderful path.

I love my parents and my younger sister. You gave me generous support and encouragement to me for a long time. I'll make you happy for my life. I am thankful to '0kcal' member, Ji-eun, Yoonjeong, Soheon, Minjung, Jiseon, and Na-yeon who have given me tremendous power for more than 7 years from the time I entered university to graduation. I wish your future will be happy from the same effort that you've studied and hardly worked. My eternal roommate, Se-yeon, Dayoung and Sohyun, I love you so much. Thank you for cheering for me always. Thanks to you guys, I was able to finish my undergraduate and master's degrees.

I want to thank everyone who knows me and helps me. I hope you to be happy and peaceful all the time.